GeroScience (2022) 44:2393–2425
https://doi.org/10.1007/s11357-022-00631-2

ORIGINAL ARTICLE

A comprehensive analysis of the mutational landscape of the newly emerging Omicron (B.1.1.529) variant and comparison of mutations with VOCs and VOIs

Chiranjib Chakraborty · Manojit Bhattacharya · Ashish Ranjan Sharma · Kuldeep Dhama · Govindasamy Agoramoorthy

Received: 8 March 2022 / Accepted: 20 July 2022 / Published online: 22 August 2022

Abstract The Omicron variant is spreading rapidly throughout several countries. Thus, we comprehensively analyzed Omicron's mutational landscape and compared mutations with VOC/VOI. We analyzed SNVs throughout the genome, and AA variants (NSP and SP) in VOC/VOI, including Omicron. We generated heat maps to illustrate the AA variants with high mutation prevalence (> 75% frequency) of Omicron, which demonstrated eight mutations with > 90% prevalence in ORF1a and 29 mutations with > 75% prevalence in S-glycoprotein. A scatter plot for Omicron and VOC/VOI's cluster evaluation was computed. We performed a risk analysis of the antibody-binding risk among four mutations (L452, F490, P681, D614) and observed three mutations (L452R, F490S, D614G) destabilized antibody interactions. Our comparative study evaluated the properties of 28 emerging mutations of the S-glycoprotein of Omicron, and the ΔΔG values. Our results showed K417N with minimum and Q954H with maximum ΔΔG value. Furthermore, six important RBD mutations (G339D, S371L, N440K, G446S, T478K, Q498R) were chosen for comprehensive analysis for stabilizing/destabilizing properties and molecular flexibility. The G339D, S371L, N440K, and T478K were noted as stable mutations with 0.019 kcal/mol, 0.127 kcal/mol, 0.064 kcal/mol, and 1.009 kcal/mol. While, G446S and Q498R mutations showed destabilizing results. Simultaneously, among six RBD mutations, G339D, G446S, and Q498R mutations increased the molecular flexibility of S-glycoprotein. This study depicts the comparative mutational pattern of Omicron and other VOC/VOI, which will help researchers to design and deploy novel vaccines and therapeutic antibodies to fight against VOC/VOI, including Omicron.

Chiranjib Chakraborty and Manojit Bhattacharya contributed equally to this work.

Supplementary Information The online version contains supplementary material available at https://doi.org/10.1007/s11357-022-00631-2.

C. Chakraborty (✉)
Department of Biotechnology, School of Life Science and Biotechnology, Adamas University, Barasat-Barrackpore Rd, Kolkata, West Bengal 700126, India
e-mail: drchiranjib@yahoo.com

M. Bhattacharya
Department of Zoology, Fakir Mohan University, Vyasa Vihar, Balasore 756020, Odisha, India

A. R. Sharma
Institute for Skeletal Aging & Orthopedic Surgery, Hallym University-Chuncheon Sacred Heart Hospital, Chuncheon-si 24252, Gangwon-do, Republic of Korea

K. Dhama
Division of Pathology, ICAR-Indian Veterinary Research Institute, Izatnagar, Bareilly 243122, Uttar Pradesh, India

G. Agoramoorthy
College of Pharmacy and Health Care, Tajen University, Yanpu, Pingtung 907, Taiwan

Keywords Omicron · Mutation · SNVs · AA variants · nAb escape

Abbreviations

AA	Amino acid
ACE2	Angiotensin-converting enzyme 2
GISAID	Global Initiative on Sharing All Influenza Data
MDS	Molecular dynamics simulation
nAb	Neutralizing antibody
NMA	Normal mode analysis
nsp	Non-structural protein
NTD	N-terminal domain
ORF	Open reading frame
RBD	Receptor binding domain
RBM	Receptor binding motif
S-glycoprotein	Spike glycoprotein
SNV	Single-nucleotide variation
UTR	Untranslated region
VOC	Variants of concern
VOI	Variants of interest
Δ	Delta

Introduction

A new SARS-CoV-2 variant, Omicron (B.1.1.529), was first identified in South Africa in November 2021 [1]. At that time, scientists noted a sudden rise in COVID-19 cases triggered by Omicron [2–4]. The variant has spread across the USA, Europe, Australia, Canada, and Hong Kong, and has spread to more than 50 countries within a few days [5–7]. Presently, the variant has spread throughout the globe, and several lineages have evolved, such as BA.1, BA.2, BA.3. BA.4, BA.5, in several countries [7–9]. Another recombinant variant, XE variant, was also reported as VOC. The recombinant XE variant contains the genomic part of BA.1 and BA.2 [10]. However, it is not currently designated as VOC by WHO [11]. Due to the Omicron variant and newly evolved lineages, the pandemic has taken a new turn.

With the sudden emergence of a new strain, the virus's evolutionary trajectory has shifted in a new direction. Generally, when a virus strain like SARS-CoV-2 creates a new line of evolution, it is called an evolutionary trajectory and might be created through positive selection [12]. Jung et al. illustrated in their article that Omicron has not originated from other VOC, and the inference was drawn from phylogenetic analysis. They have also illustrated the amino acid changes that occurred through positive selection pressure [13]. Meanwhile, several lineages have evolved from Omicron [7–9]; thus, Omicron has also created an evolutionary trajectory. Scientists and policymakers are searching for strategies to fight against variants [14, 15]. Through research, they are trying to understand the properties of variants, such as immune escape, antibody escape, and vaccine escape [16, 17]. A recent study by Zhang et al. shows that the Omicron variant exhibits a severe immune escape from the convalescent sera collected from COVID-19 patients. They illustrated that the Omicron variant could escape the neutralized convalescent sera collected in patients infected with the Delta variant or previous strains [18].

The variants have the highest mutations compared to other variants; therefore, it is necessary to understand the impacts of the variants due to their highest mutational load. Quarleri et al. have studied the effect of the high mutational load, and they discussed the mutations in RBD, the S-glycoprotein other than the RBD region, nucleocapsid (N), and deletion in ORF1a [19]. Similarly, Kumar et al. performed a comparative analysis between Omicron and Delta variants of the S-glycoprotein. The relative binding affinity was evaluated using a docking study between the RBD of the S-glycoprotein and the hACE2 receptor in three strains (wild type, Delta, and Omicron variants) to understand the binding affinity with the hACE2 receptor. The docking result showed that the Omicron variant is more likely to interact with hACE2 than the Delta variant. Thus, the Omicron variant has a higher possibility of transmission [20]. It is, therefore, essential to understand all mutations at the molecular level, including their characteristics of mutations. Pascarella et al. assessed the electrostatic potential between the Omicron variant and S-glycoprotein's other two VOCs (Delta and Delta-plus variants). They evaluated the increased electrostatic potential of the Omicron variant compared to the Delta and Delta-plus variants and indicated that the electrostatic potential favored higher transmissibility leading to augmented infectivity [21]. Recently, the XE variant has been spreading worldwide; this is a recombinant variant of the two sub-variants of Omicron and, therefore, a recombinant variant of BA.1 and BA.2. In addition to the XE variant, two

other recombinant variants, XD and XF, have recently emerged [22, 23].

The spread of this recent variant worldwide has created a global concern. Therefore, more understanding and research data are necessary about the molecular determinant factors, such as emerging mutations that provide the Omicron variant's spreading capacity. Scott et al. suggested capturing data at the molecular level during the spread of this variant. They provided examples, such as collecting S-gene data during the variant from the genome sequence of its different strains. The S-gene data of the Omicron variant may help understand the degree of vaccine escape or the escape from the immune systems of vaccinated individuals [24]. Therefore, it is urgent to unfold all mutations at the molecular level in the Omicron variant, some of which are escape mutations, to help overcome phenomena such as antibody escape and to compare them with the other VOCs and VOIs.

Studies have shown that the Omicron variant has accumulated approximately 50 mutations in different regions of its genome, out of which, 32 mutations have been observed throughout the spike-glycoprotein [20, 25–27]. Preliminary studies have pointed out several overlapping muttons from the other VOCs and VOIs, including Delta, Alpha, Gamma, Beta, Mu, and Lambda. Some overlapping mutations from VOCs or VOIs are N501Y, T478K, N655Y, D614G, N679K, and P681H [28–32]. Therefore, it is crucial to understand the frequency of mutations Omicron variant and compare them with the mutation variants of present VOCs and VOIs.

Notably, some mutations in the spike-glycoprotein are responsible for antibody escape, especially mutations in the RBD region [33, 34]. Therefore, it is essential to map significant mutations from the RBD region that are responsible for escape properties in Omicron and to characterize the molecular and mutational properties of these RBD mutations.

Variants such as Delta (B.1.617.2), Alpha (B.1.1.7), Gamma (P.1), Beta (B.1.351), and Omicron are emerging variants of SARS-CoV-2 that are entitled as variants of concern (VOC) by WHO, CDC (USA), and ECDC (EU) due to some changes compared to the wild type of the Wuhan strain. The differences noted include the increase in virulence or adaptation in clinical disease presentation and an increase in transmissibility [28–30]. Lambda (C.37) and Mu (B.1.621) are entitled variants of interest (VOI). However, WHO categorizes variants as VOCs or VOIs based on their present virulence pattern or pattern change in clinical disease presentation and transmissibility pattern. The status level of VOC or VOI of any variant can be changed. In this study, we analyzed the mutational landscape of Omicron along with the VOCs and VOIs. We considered those variants to be VOCs and VOIs concerning their current status.

In this study, we attempted to comprehend the mutational landscape of the Omicron variant and compare the mutations with those of others. We illustrated single-nucleotide variations (SNVs) throughout the Omicron genome and compared the mutations with other VOCs and VOIs. We also analyzed amino acid (AA) variants in Omicron's non-structural proteins (NSPs) and other VOCs and VOIs. We also generated heat maps to illustrate the AA variants with a high mutation prevalence (> 75% mutational frequency) in Omicron and other variants. Our study attempted to explain Omicron's antibody/nAb escape phenomenon and other VOCs and VOIs. A comparative study evaluated the molecular and mutational properties of 28 emerging mutations of the S-glycoprotein of Omicron, and the ΔΔG values were calculated. Furthermore, we chose six important RBD mutations (G339D, S371L, N440K, G446S, T478K, and Q498R) of Omicron and other variants for further comprehensive analysis of the molecular and mutational properties that may be responsible for antibody/nAb escape and partial vaccine escape.

Methods

Data collection of the mutational landscape of the Omicron variant and other VOCs and VOIs

Data associated with the Omicron variant and other VOCs and VOIs were collected from several databases using search engines. We retrieved meaningful information from literature on the SARS-CoV-2 Omicron and other variants from databases such as Web of Science [35], Google Scholar [36], and PubMed [37, 38]. We collected data on the Omicron variants and other VOCs/VOIs from the CDC, ECDC, and WHO [39–42].

We obtained information on the Omicron variants and other VOCs/VOIs from the GISAID database

[43, 44] and retrieved data from the RCSBPDB database as PDB files to develop modes for the S-glycoprotein/S-glycoprotein-antibody interactions [45].

Data analysis of the mutational landscape of the Omicron variant and other VOCs and VOIs

Data analysis of the mutation of Omicron variant and other VOCs and VOIs

We applied computational tools, servers, and software to explain the mutational landscape of the Omicron variant and the current VOCs and VOIs. Using PyMOL software, we developed different 3D structural models of the Omicron variant, other VOCs, and VOIs [46, 47]. We used the COVID-19 CG server [48], Nextstrain server [49], Nextstrain (2021)[50], and Outbreak.info [51] for further analysis. For the analysis of SNVs in the Omicron genome, along with other VOCs and VOIs, we used the COVID-19 CG server [48]. For AA variants in the non-structural and structural proteins of Omicron and other VOCs and VOIs, we used the COVID-19 CG server [48]. We used Outbreak.info [51] to provide the heat map-like representation of the high mutation (AA mutation) prevalence (> 75% mutational frequency) of Omicron and other VOCs and VOIs. The Nextstrain server was used to develop a scatter plot for VOCs and VOIs. A 3D model of the S-glycoprotein using PyMOL software and the emerging mutations for antibody interaction were depicted for the Omicron variant, other VOCs, and VOIs [46, 47]. VarEPS was used to analyze emerging mutations related to risk analysis of mutations for antibody-binding, antibody binding sites, and risk analysis of important mutations [52].

The comprehensive prediction of some properties of 28 mutations, including G339D, S371L, N440K, G446S, T478K, and Q498R in the S-glycoprotein of Omicron

We have selected 28 mutations of Omicron's S-glycoprotein to predict the mutation properties for this study. Researchers widely accept these mutations, and published literature is also available for these mutations from emerging Omicron mutational variants.

We used the DynaMut server to evaluate the 28 mutations in the S-glycoprotein and its characteristic effect [53]. Here, we analyzed several mutation properties (stabilizing/destabilizing events and decreasing molecular flexibility). Properties like fluctuation, interatomic interactions, and deformation of an AA because of a mutation can be represented by the ΔΔG of DDG (Delta-Delta G). The DDG of the AA point mutations of the S-glycoprotein of Omicron were computed to understand its thermodynamic stability. The server illustrated the point mutation into two categories: stabilizing events (ΔΔG value was described as ≥ 0) and destabilizing events (ΔΔG was illustrated as < 0) [53]. Capriotti et al. showed a similar value of the ΔΔG to categorize the point mutations using the stabilizing/destabilizing state [54].

Depiction of plot, graphs, and statistical models

Statistical software (PAST 4.03) was used to generate statistical models [55]. Simultaneously, we used MATLAB to represent the graphs and plots whenever needed [56]. A flow diagram is portrayed to provide an overview of our study to comprehend the mutation mapping of the Omicron variant (Fig. 1A). In addition, the location of the six selected mutations in the S-glycoprotein in our study has been depicted (Fig. 1B).

Results

Mutational landscape of Omicron variant and comparison with the mutations of other VOCs and VOIs

We illustrated the mutational landscape of Omicron and compared the mutations with those of other VOCs. First, a schematic diagram representing all the mutational landscapes throughout the genome and its comparison with VOCs and VOIs was created (Fig. 2A). Our study corroborates previous findings about the immense number of mutations in the Omicron genome compared to other variants. We developed a statistical model using the total number of mutations in the genome. It shows the number of mutations of different VOCs (Alpha, Delta, Gamma, and Beta) and VOIs (Lambda, Mu). In this model, we found all the VOCs and VOIs, including Alpha, Delta, Gamma, Beta, Lambda, and Mu, in a cluster showing the number of mutations

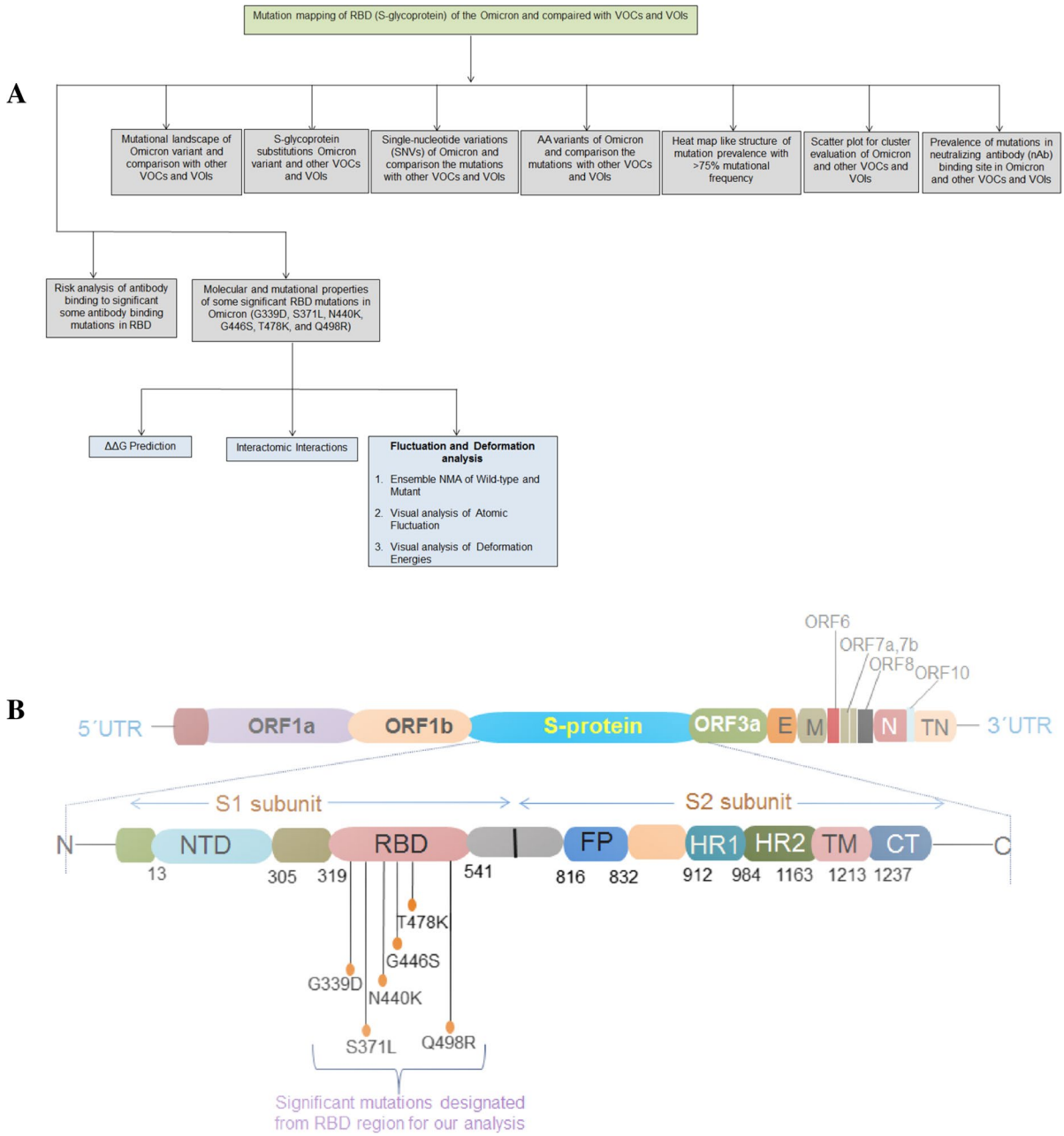

Fig. 1 A flow diagram shows the graphical view of our study overall. It also shows the graphic demonstration of the emerging selected mutations from (**A**) A flow diagram of our study to evaluate the mutational landscape of the Omicron (B.1.1.529) variant. (**B**) A schematic diagram shows the location of the selected six mutations from the RBD regions of the S-glycoprotein for our study. The study analyzed the molecular and mutational properties of 28 significant mutations, including G339D, S371L, N440K, G446S, T478K, and Q498R

other than Omicron. The variant is out of cluster due to more mutations (Fig. 2B). However, from this model, we found that the clustering event formed two groups: the first containing all variants and the second containing only Omicron. Omicron exhibits a high number of mutation patterns compared to

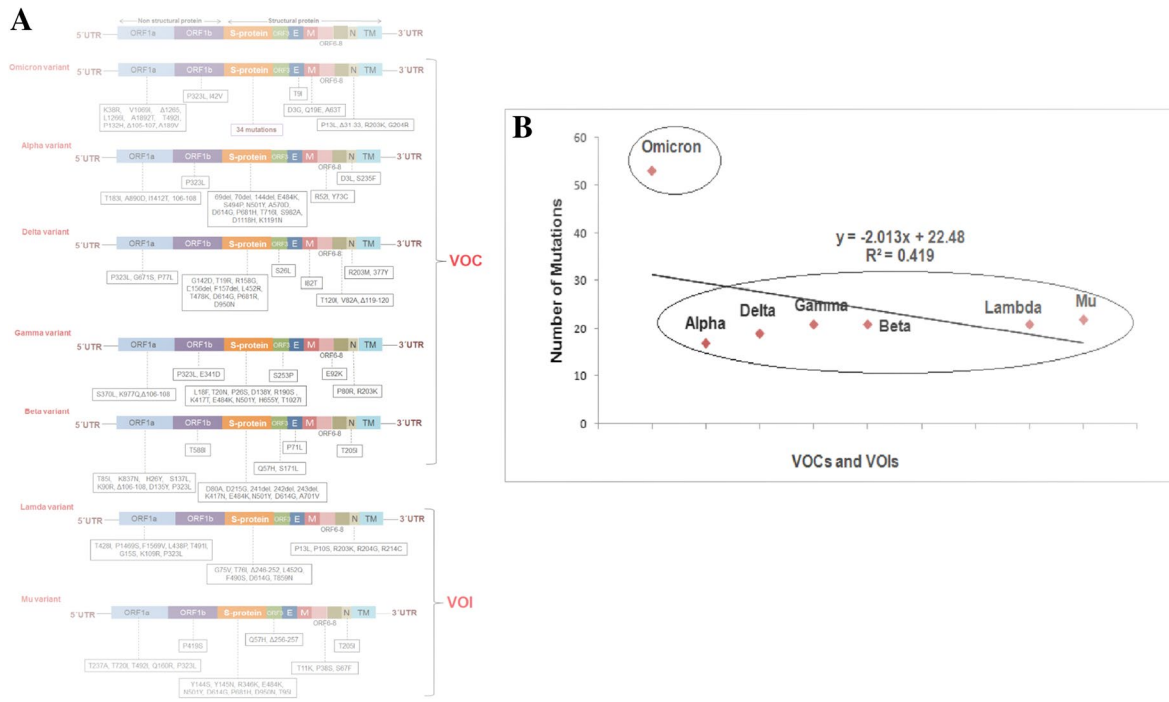

Fig. 2 A schematic diagram representing the mutational landscape throughout the genome of Omicron and its comparison with VOCs and VOIs. (**A**) The mutational landscape throughout the genome of Omicron and its comparison with VOCs and VOIs. (**B**) A statistical model illustrates the number of total genome mutations in the VOCs and VOI, including Omicron. This model shows the number of mutations in the genome of VOCs and VOIs Alpha, Delta, Gamma, Beta, Lambda, and Mu formed a cluster regarding the number of mutations. Here, the clustering event formed two groups: The first one contains all variants, and the second one is Omicron. Omicron exhibits a high number of mutation patterns compared to other VOCs and VOIs. For the analysis, we have taken the data from the literature collected from open source databases such as Google Scholar [36] and PubMed [37, 38]. At the same time, we also collected the open source mutation information on CDC's Omicron variants and other VOCs/VOIs [39–41]; eCDC[41], WHO[42] etc.

other VOCs and VOIs. The mutational landscape of the Omicron variant is presented in Table 1.

S-glycoprotein substitutions in the Omicron variant and other VOCs and VOIs

We illustrated the mutational landscape of the Omicron S-glycoprotein. A schematic diagram represents all mutational landscapes throughout the genome and its comparison with VOCs and VOIs (Fig. 3A). We constructed a statistical model using the total number of mutations in the S-glycoprotein. The model showed that all VOCs and VOIs formed a cluster other than Omicron (Fig. 3B). Here, the clustering event also formed two groups: the first group contained all variants and the second group contained only Omicron. Similar to the previous model (developed using the number of total genome mutations), Omicron belongs to a different group and shows a different pattern than other variants regarding the number of mutations.

The 3D model deployment of the S-glycoprotein with mutations is significant for the SARS-CoV-2 variant, providing an interactive platform. A 3D model was generated using bioinformatics. The 3D model helps to compare the protein with other variants using 3D space. We developed a 3D model to understand the position of all mutations of S-glycoprotein, the Omicron, and other VOCs and VOIs. Every model was generated to understand every detail of the mutational landscape of the Omicron and other VOCs and VOIs (Alpha, Delta, Gamma, Beta, Lambda, and Mu). We identified mutations of the S-glycoprotein of Omicron in a 3D model (Fig. 4A). Mutations in the RBD of the S-glycoprotein of Omicron were depicted

Table 1 Mutational landscape of Omicron variant

Mutation	Mutation site	Remarks
A67V	NTD of Spike protein	Ala $\overset{67}{\rightarrow}$ Val
Δ69–70	Spike protein deletion	Deletion mutations
T95I	NTD of Spike protein	Thr $\overset{95}{\rightarrow}$ Ile
G142D	NTD of Spike protein	Gly $\overset{142}{\rightarrow}$ Asp
Δ143–145	Spike protein deletion	Deletion mutations
Δ211	Spike protein deletion	Deletion mutations
L212I	NTD of Spike glycoprotein	Leu $\overset{212}{\rightarrow}$ Ile
ins214EPE	Insertion in Spike glycoprotein	Insertions of Glu, Pro, and Glu amino acids
T547K	Spike glycoprotein	Thr $\overset{547}{\rightarrow}$ Lys
D614G	Spike glycoprotein	Asp $\overset{614}{\rightarrow}$ Gly
H655Y	Spike glycoprotein	His $\overset{655}{\rightarrow}$ Tyr
N679K	Spike glycoprotein	Asn $\overset{679}{\rightarrow}$ Lys
P681H	Spike glycoprotein	Pro $\overset{681}{\rightarrow}$ His
N764K	Spike glycoprotein	Asn $\overset{764}{\rightarrow}$ Lys
D796Y	Fusion peptide in Spike protein	Asp $\overset{796}{\rightarrow}$ Tyr
N856K	Spike glycoprotein	Asn $\overset{856}{\rightarrow}$ Lys
Q954H	HR1 in Spike protein	Gln $\overset{954}{\rightarrow}$ His
N969K	HR1 in Spike protein	Asn $\overset{969}{\rightarrow}$ Lys
L981F	HR1 in Spike protein	Leu $\overset{981}{\rightarrow}$ Phe
G339D	RBD in Spike protein	Gly $\overset{339}{\rightarrow}$ Asp
S371L	RBD in Spike protein	Ser $\overset{371}{\rightarrow}$ Leu
S373P	RBD in Spike protein	Ser $\overset{373}{\rightarrow}$ Pro
S375F	RBD in Spike protein	Ser $\overset{375}{\rightarrow}$ Phe
K417N	RBD in Spike protein	Lys $\overset{417}{\rightarrow}$ Asn
N440K	RBD in Spike protein	Asn $\overset{440}{\rightarrow}$ Lys
G446S	RBD in Spike protein	Gly $\overset{446}{\rightarrow}$ Ser
S477N	RBD in Spike protein	Ser $\overset{477}{\rightarrow}$ Asn
T478K	RBD in Spike protein	Thr $\overset{478}{\rightarrow}$ Lys
E484A	RBD in Spike protein	Glu $\overset{484}{\rightarrow}$ Ala
Q493K	RBD in Spike protein	Gln $\overset{493}{\rightarrow}$ Lys
G496S	RBD in Spike protein	Gly $\overset{496}{\rightarrow}$ Ser
Q498R	RBD in Spike protein	Gln $\overset{498}{\rightarrow}$ Arg
N501Y	RBD in Spike protein	Asn $\overset{501}{\rightarrow}$ Tyr
Y505H	RBD in Spike protein	Tyr $\overset{505}{\rightarrow}$ His
K38R	ORF1a	Lys $\overset{38}{\rightarrow}$ Arg
V1069I	ORF1a	Val $\overset{1069}{\rightarrow}$ Ile
Δ1265	Deletion in ORF1a	Deletion mutation
L1266I	ORF1a	Leu $\overset{1266}{\rightarrow}$ Ile

Table 1 (continued)

Mutation	Mutation site	Remarks
A1892T	ORF1a	Ala $\overset{1892}{\rightarrow}$ Thr
T492I	ORF1a	Thr $\overset{492}{\rightarrow}$ Ile
P132H	ORF1a	Pro $\overset{132}{\rightarrow}$ His
Δ105–107,	Deletions in ORF1a	Deletion mutations
A189V	ORF1a	Ala $\overset{189}{\rightarrow}$ Val
P323L	ORF1b	Pro $\overset{323}{\rightarrow}$ Leu
I42V	ORF1b	Ile $\overset{42}{\rightarrow}$ Val
T9I	Envelope protein	Thr $\overset{9}{\rightarrow}$ Ile
D3G	Nucleoprotein	Asp $\overset{3}{\rightarrow}$ Gly
Q19E	Nucleoprotein	Gln $\overset{19}{\rightarrow}$ Glu
A63T	Nucleoprotein	Ala $\overset{63}{\rightarrow}$ Thr
P13L	Nucleocapsid protein	Pro $\overset{13}{\rightarrow}$ Leu
Δ31–33	Deletions in Nucleocapsid protein	Deletion mutations
R203K	Nucleocapsid protein	Arg $\overset{203}{\rightarrow}$ Lys
G204R	Nucleocapsid protein	Gly $\overset{204}{\rightarrow}$ Arg

using a 3D model. We found 15 mutations in the RBD region (Fig. 4B). Mutations in the RBM of the S-glycoprotein of Omicron were depicted using a 3D model. We found ten mutations in the RBM region (Fig. 4C). Simultaneously, all mutations of the S-glycoprotein of VOCs (Alpha, Delta, Gamma, and Beta) have been illustrated (Fig. 4D). Mutations of Omicron are a puzzle for researchers, and they have attempted to solve these mutations [54]. Our study is significant in this regard. However, this part of the analysis will assist researchers in understanding the Omicron mutations and those of the Alpha, Delta, Gamma, and Beta variants. The 3D molecular statures of Omicron may help elucidate global takeover events [57]. This structural basis of understanding the Spike protein SARS-CoV-2 will help future researchers further understand this variant's functional properties. This study informs us of emerging mutations in 3D, and it will assist future researchers in understanding emerging mutations such as E484K, K417T, N501Y, S494P, and L452R for functionality mapping.

All the mutations of the RBD of VOCs (Alpha, Delta, Gamma, and Beta) were identified under the particular position of mutations (Fig. 4E). Similarly, a 3D model was developed to comprehend all mutations of the S-glycoprotein of the VOIs (Lambda and Mu) (Fig. 4F). We illustrated the understanding of all RBD mutations of the S-glycoprotein in the VOIs (Fig. 4G). The mutational landscape for the mutations of the S-glycoprotein has been illustrated for all the VOCs using a table (Table 2). The mutational landscape for the important mutations of the S-glycoprotein has been illustrated for the VOIs in Table 3.

Single-nucleotide variations (SNVs) of 5'UTR, ORF1a, ORF1ab, S, ORF3a, E, M, ORF6, ORF7a, ORF7b, ORF8, N, and 3′UTR regions of Omicron and comparison other VOCs and VOIs

We analyzed SNVs throughout the genome (including 5′UTR, ORF1a, ORF1ab, S, ORF3a, E, M, ORF6, ORF7a, ORF7b, ORF8, N, and 3′UTR regions) of Omicron and compared them with other VOCs and VOIs.

A comparative analysis of SNVs of the 5′UTR region is illustrated in Fig. 5A. We found that SNV with the highest mutational frequency was C241T. For Omicron, the mutational frequency was 94%. However, the mutational frequency was noted in the case of Delta (99%), Alpha (100%), Beta (100%), Gamma (99%), Lambda (100%), and Mu (99%).

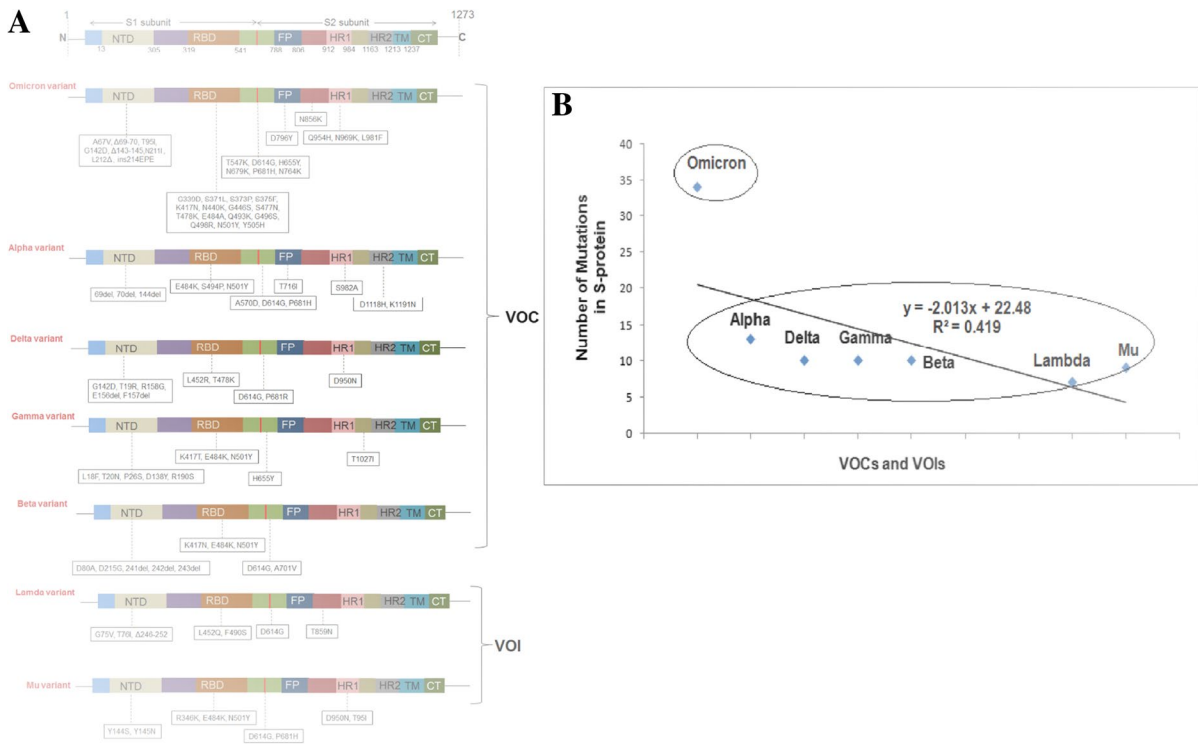

Fig. 3 A schematic diagram represented the mutational landscape throughout the S-glycoprotein of Omicron and its comparison with VOCs and VOIs. (**A**) The mutational landscape throughout the S-glycoprotein of Omicron and its comparison with VOCs and VOIs. (**B**) A statistical model demonstrates the number of mutations in the S-glycoprotein in the VOCs and VOI, including Omicron. This model shows the number of mutations in the S-glycoprotein of VOCs and VOIs Alpha, Delta, Gamma, Beta, Lambda, and Mu formed a cluster regarding the number of mutations. Here, the clustering event also formed two groups: The first one contains all variants, and the second one is Omicron. Like the previous model (developed using the number of total genome mutations), Omicron belongs to a different group and shows a different pattern compared to other variants in terms of the number of mutations. For the analysis, we have taken the data from the literature collected from open source databases such as Google Scholar [36], PubMed[37, 38] etc. At the same time, we also collected the open source mutation information on CDC's Omicron variants and other VOCs/VOIs [39–41]; eCDC [41], WHO[42] etc.

Similarly, a comparative analysis of SNVs in the ORF1a region is illustrated in (Fig. 5B), showing that SNV with the highest mutational frequency was C3037T. For Omicron, the mutational frequency was 93%. It was 100% for all other VOCs and VOIs.

The comparative analysis of SNVs of the ORF1ab region revealed that the two SNVs with the highest mutational frequencies were C3037T and C14408T (Fig. 5C). For Omicron, the mutational frequencies of these SNVs were 94% and 98%, respectively. However, SNV C3037T was 100% for other VOCs and VOIs. Similarly, the SNV C14408T was 100% for Delta, 100% for Alpha, 90% for Beta, 98% for Gamma, 100% for Lambda, and 99% for Mu.

The comparative analysis of SNVs in the S region is illustrated (Fig. 5D). We found that the SNV with the highest mutational frequency was A23403G. For Omicron, the mutational frequency was 99%. However, it was noted as 100% for all other VOCs and VOIs.

The comparative analysis of SNVs in the ORF3a region is illustrated in Fig. 5E. It was observed that the SNV with the highest mutational frequency of SNV is A23403G. In the case of Omicron, the mutational frequency of the SNV was 99%. It was noted as 100% for all other VOCs and VOIs.

We evaluated the SNVs of the E region (Fig. 5F). We found only one SNV (A26270G) in Omicron, with a mutational frequency of 81%. The SNV was not found for other variants.

For the M region, we found three SNVs for Omicron, A26530G, C26577G, and G26709A, and the

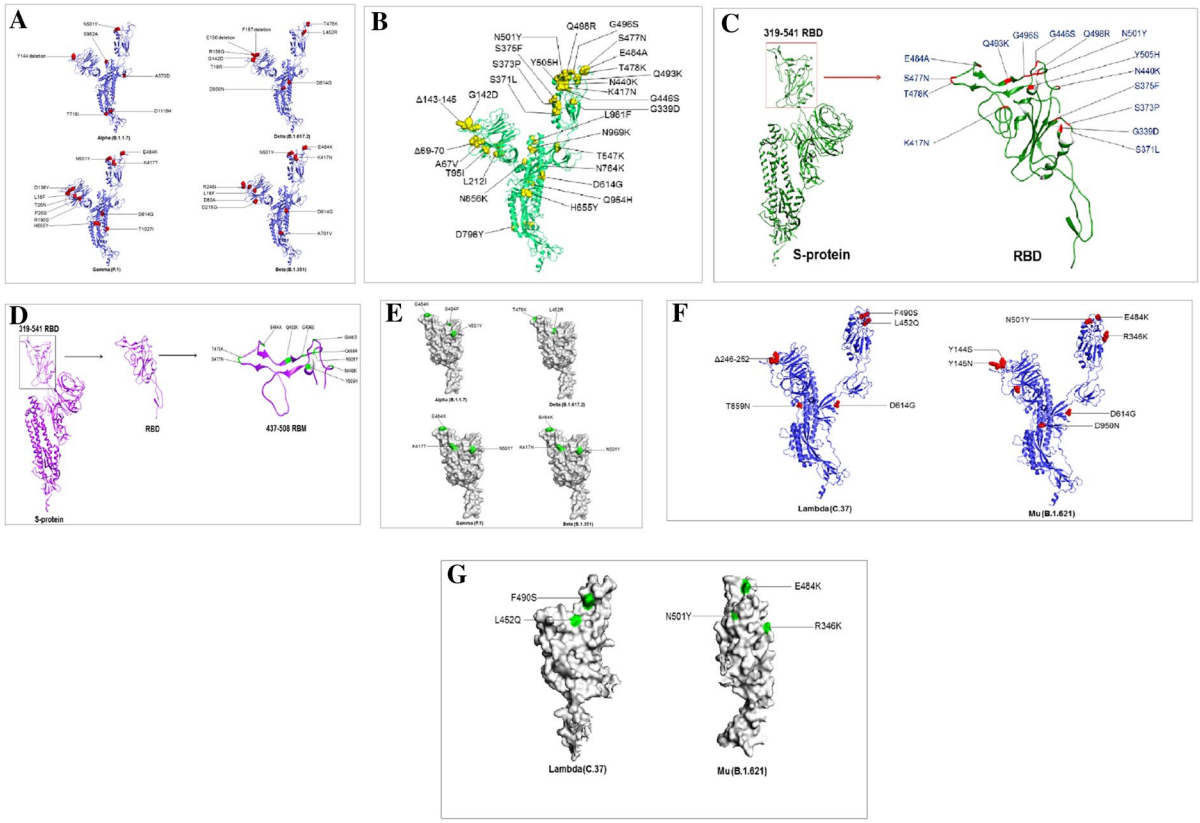

Fig. 4 3D model illustrated the mutational landscape throughout the S-glycoprotein of Omicron and its comparison with VOCs and VOIs. (**A**) A 3D model that illustrates all the mutations of the S-glycoprotein of Omicron. (**B**) A 3D model that illustrates all the mutations RBD region of the S-glycoprotein of Omicron. (**C**) A 3D model describes all the mutations RBM of the S-glycoprotein of Omicron. (**D**) A 3D model that illustrates all the mutations in the VOCs (Delta (B.1.617.2), Alpha (B.1.1.7), Gamma (P.1), Beta (B.1.351)). (**E**) A 3D model that illustrates all the RBD mutations in the VOCs (Delta (B.1.617.2), Alpha (B.1.1.7), Gamma (P.1), Beta (B.1.351)). (**F**) A 3D model that illustrates all the mutations in the VOIs (Lambda (C.37) and Mu (B.1.621). (**G**) A3D model that illustrates all the RBD mutations in the VOIs (Lambda (C.37) and Mu (B.1.621)). All the 3D models were developed using PyMOL software. For a 3D model generation, we used some PDB files (PDB ID: 6VXX)

mutational frequencies were 41%, 73%, and 90%, respectively (Fig. 6A). SNV T26767T was also found for Delta with an SNV of 100%.

Only one mutational frequency (91%) was found for Omicron for SNV A27259C (Fig. 6B). For the ORF7a region, we found two SNVs. However, the mutational frequencies were insignificant, and these two SNVs could not be considered (Fig. 6C). Here, we found two SNVs for the Delta variant, T27638C, and C27752T, and the mutational frequencies were the same (97%) in both cases. For the ORF7b region, SNV C27807T was found in Omicron, and the mutational frequency was 66% (Fig. 6D). Another SNV C27874T with a mutational frequency of 77% was identified in Delta variant in this region.

In the ORF78 region, we found no significant SNVs for Omicron (Fig. 6E). Here, we identified three SNVs with the highest mutational frequencies for Alpha (C27972T, G28048T, and A28111G), with mutational frequencies of 99% for all SNVs. We also found the two highest mutational frequencies for Mu (C27925A and C28005T), with mutational frequencies of 99% each. For the M region, the two significant SNVs for Omicron (> 75%) were C28311T and G28881A, with mutational frequencies of 80% and 78%, respectively (Fig. 6F).

Table 2 Emerging mutations in S-protein of VOCs of SARS-CoV-2

Sl No	SARS-CoV-2 VOC	Variants name (WHO label)	SARS-CoV-2 lineages	Mutations in S-protein	
				RBD region	Other than the RBD region
1	21 K, GR/484A	Omicron	B.1.1.529	G339D, S371L, S373P, S375F, K417N, N440K, G446S, S477N, T478K, E484A, Q493K, G496S, Q498R, N501Y, Y505H	A67V, Δ69–70, T95I, G142D, Δ143–145, Δ211, L212I, ins214EPE,T547K, D614G, H655Y, N679K, P681H, N764K, D796Y, N856K, Q954H, N969K, L981F
2	20I/501Y.V1	Alpha	B.1.1.7	E484K, S494P, N501Y	69del, 70del, 144del, A570D, D614G, P681H, T716I, S982A, D1118H, K1191N
3	21A, 21I, 21 J/20A/S:478 K	Delta	B.1.617.2	L452R, T478K	G142D, T19R, R158G, D614G, P681R, D950N, E156del, F157del
4	20 J/501Y.V3	Gamma	P.1	K417T, E484K, N501Y	L18F, T20N, P26S, D138Y, R190S, H655Y, T1027I
5	20H/501Y.V2	Beta	B.1.351	K417N, E484K, N501Y	D80A, D215G, 241del, 242del, 243del, D614G, A701V

Lastly, the 3′UTR region analysis showed no significant SNVs for Omicron (Fig. 6G). However, we found one highly significant SNV for the Delta variant, G29742T, with a mutational frequency of 99%. However, we have tried to analyze mutational study events of ORF6. Nevertheless, the used server failed to generate the mutational event.

Recently, Yadav et al. found the Omicron variant in collected samples, and the genome was analyzed using next-generation sequencing. Finally, several SNVs were found in Omicron clinical isolates [58]. Ahmed et al. found the Omicron variant by sequencing a swab sample collected from the nasopharynx of an aircraft traveler. The Omicron variant was also found in subsequent sequencing (ATOPlex and Nanopore) of aircraft wastewater samples. They have attempted to discuss the genome in light of SNVs. However, researchers have not yet fully analyzed SNVs [59]. However, we performed a comprehensive SNV analysis throughout the genome of Omicron and compared it with other VOCs/VOIs.

Amino acid (AA) variants in the non-structural proteins of Omicron and comparison with mutations in other VOCs and VOIs

We analyzed AA variants in the non-structural proteins (nsp2, nsp3 (PL2-PRO), nsp4, nsp5 (3CLp), nsp6, nsp12 (RdRp), nsp13 (Helicase), and nsp14) of Omicron and compared the mutations with other VOCs and VOIs. No AA variant was found in the Omicron region of nsp2 (Fig. 7A). We found a T85I AA variant with 100% mutational frequency in the Delta variant. Similarly, in nsp3, the maximum mutational frequency of the Omicron variant was 78% in the A1892T AA variant (Fig. 7B). We found a highly significant mutational frequency of the AA variant in three places in the Alpha variant as well, which was 100% at T183I and A890D and 99% at I1412T. We also found the Mu variant mutational frequency of 100% in T720I AA. In nsp4, one AA variant had a significant mutational frequency (99%) among the Omicron variant in T492I (Fig. 7C). Lambda had two

Table 3 Emerging mutations in S-protein of SARS-CoV-2 VOIs

Sl no	Significant SARS-CoV-2 variants	Variants name (WHO label)	SARS-CoV-2 lineages	Mutations in S-protein	
				RBD region	Other than the RBD region
1	21G	Lambda	C.37	L452Q, F490S	G75V, T76I, Δ246–252, D614G, T859N
2	21H	Mu	B.1.621	R346K, E484K, N501Y	T95I, Y144S, Y145N,D614G, P681H, D950N

Fig. 5 Single-nucleotide variations (SNVs) of some parts of the genome (5′UTR, ORF1a, ORF1ab, S, ORF3a, E) of Omicron along with other VOCs and VOIs. (**A**) SNVs of 5′UTR of Omicron along with other VOCs and VOIs. (**B**) SNVs of ORF1a of Omicron along with other VOCs and VOIs. (**C**) SNVs of ORF1ab of Omicron along with other VOCs and VOIs. (**D**) SNVs of S of Omicron along with other VOCs and VOIs. (**E**) SNVs of ORF3a of Omicron along with other VOCs and VOIs. (**F**) SNVs of E of Omicron along with other VOCs and VOIs. We have used the COVID-19 CG server for SNVs analysis of these parts of the genome (5′UTR, ORF1a, ORF1ab, S, ORF3a) (**E**) of Omicron along with other VOCs and VOIs [48]. The server used the data from the GISAID ingestion pipeline, which is open-source data [48]

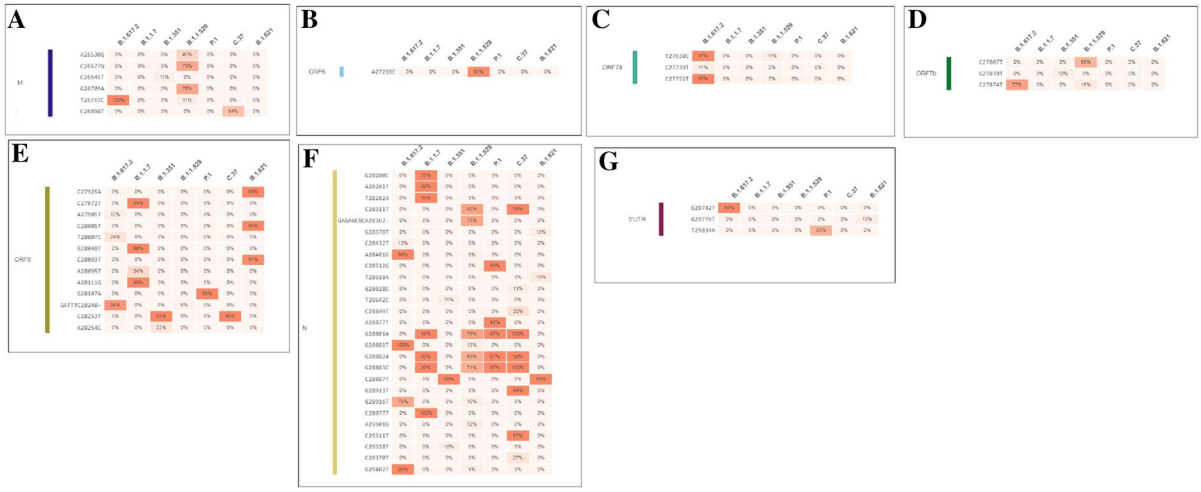

Fig. 6 Single-nucleotide variations (SNVs) of some other parts of the genome (M, ORF6, ORF7a, ORF7b, ORF8, 3′UTR) of Omicron along with other VOCs and VOIs. (**A**) SNVs of M of Omicron along with other VOCs and VOIs. (**B**) SNVs of ORF6 of Omicron, along with other VOCs and VOIs. (**C**) SNVs of ORF7a of Omicron, along with other VOCs and VOIs. (**D**) SNVs of ORF7b of Omicron, along with other VOCs and VOIs. (**E**) SNVs of ORF8 of Omicron, along with other VOCs and VOIs. (**F**) SNVs of N of Omicron along with other VOCs and VOIs. (**G**) SNVs of 3′UTR of Omicron along with other VOCs and VOIs. We have also used the COVID-19 CG server for SNVs analysis of these parts of the genome (M, ORF6, ORF7a, ORF7b, ORF8, 3′UTR) of Omicron along with other VOCs and VOIs [48]. The server used the data from the GISAID ingestion pipeline, which is open-source data [48]

AA variants (L438P and T492I) with 100% mutational frequency. Similarly, Mu has one AA variant (T492I) with 100% mutational frequency. In nsp5, we found one AA variant (P132H) with an 83% mutational frequency in the Omicron variant (Fig. 7D). Additionally, we found one AA variant (K90R) with 99% mutational frequency in the Beta variant and one AA variant (G15S) had 97% mutational frequency in the Lambda variant. Similarly, in nsp6, Omicron had one AA variant (I189V) with an 88% mutational

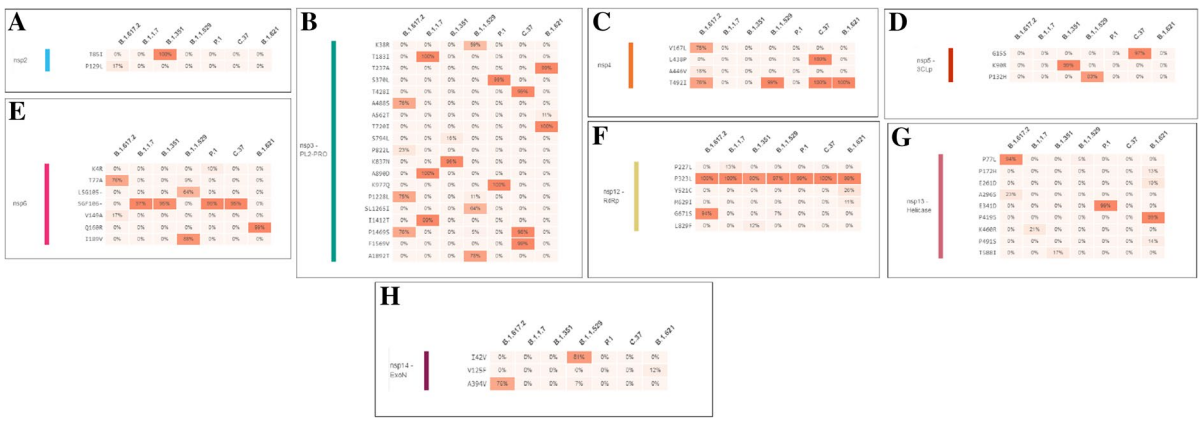

Fig. 7 Amino acid (AA) variants in the non-structural proteins of Omicron along with other VOCs and VOIs. (**A**) AA variants in nsp2, (**B**) AA variants in nsp-3 (PL2-PRO), (**C**) AA variants in nsp4, (**D**) AA variants in nsp5(3CLp), (**E**) AA variants in nsp6, (**F**) AA variants in nsp12 (RdRp), (**G**) AA variants in nsp13 (Helicase), (**H**) AA variants in nsp14. In this part of the study, we have also used the COVID-19 CG server to analyze the amino acid (AA) variants of non-structural proteins of Omicron along with other VOCs and VOIs [48]. The server used the data from the GISAID ingestion pipeline, which is open-source data [48]

frequency (Fig. 7E). We also found one AA variant (Q160R) with a 99% mutational frequency in the Lambda variant.

In nsp12, we found one AA variant (P323L) with a significant mutational frequency for VOCs and VOIs, including Omicron (Fig. 7F). Mutational frequencies were 100% (Delta), 100% (Alpha), 90% (Beta), 97% (Omicron), 100% (Lambda), and 99% (Mu). However, no AA variant was found in Omicron in the nsp13 region (Fig. 7G). Delta had one AA variant (P77L) with a significant mutational frequency of 94%. Similarly, Mu had one AA variant (P419S) with a mutational frequency of 99%. In contrast, one AA variant was found with a mutational frequency of 81% in Omicron in the nsp114 region (Fig. 7H).

3.5. Amino acid (AA) variants of structural proteins and associated regions (S-glycoprotein, ORF3a, ORF3b, E, M, ORF7a, ORF7b, ORF8, N, ORF9b, and ORF9c) of Omicron and comparison with mutations in other VOCs and VOIs

We evaluated AA variants in structural proteins and associated regions (S-glycoprotein, ORF3a, ORF3b, E, M, ORF7a, ORF7b, ORF8, N, ORF9b, and ORF9c) of Omicron and compared the mutations with other VOCs and VOIs. We found several AA variants in the S-glycoprotein with significant mutational frequency in Omicron. The AA variants with mutational frequency are A67V (75%), HV69 (66%), T95I (84%), GVYY142D (71%), T478K (69%), T547K (74%), D614G (99%), H655Y (91%), N679K (91%), P681H (91%), N764K (63%), D796Y (71%), N856K (74%), Q954H (86%), N969K (81%), L981F (81%), G339D (58%), S371L (40%), S373P (42%), S375F (43%), K417N (26%), N440K (34%), G446S (33%), S477N (40%), T478K (69%), E484A (42%), Q493K (43%), G496S (39%), Q498R (43%), N501Y (44%), and Y505H (43%). Interestingly, one AA variant (D614G) was mutated in all VOCs and VOIs, including Omicron (Fig. 8A). Mutation frequencies were 100% (Delta), 100% (Alpha), 100% (Beta), 99% (Omicron), 100% (Lambda), and 100% (Mu).

In ORF3a, no AA variant was detected in the Omicron (Fig. 8B). We found S26L (Delta) and Q57H (Mu) AA variants with a 100% mutational frequency. In orf3a, one AA variant (P21S) had a significant mutational frequency (94%) in the Omicron variant (Fig. 8C).

One AA variant (T9I) with 82% mutational frequency was found in Omicron in the M protein (Fig. 8D). Similarly, three AA variants (D3G, Q19E, and A63T) with 39%, 69%, 72% mutational frequencies were found in Omicron in the M protein (Fig. 8E). Simultaneously, one AA variant (I82T)

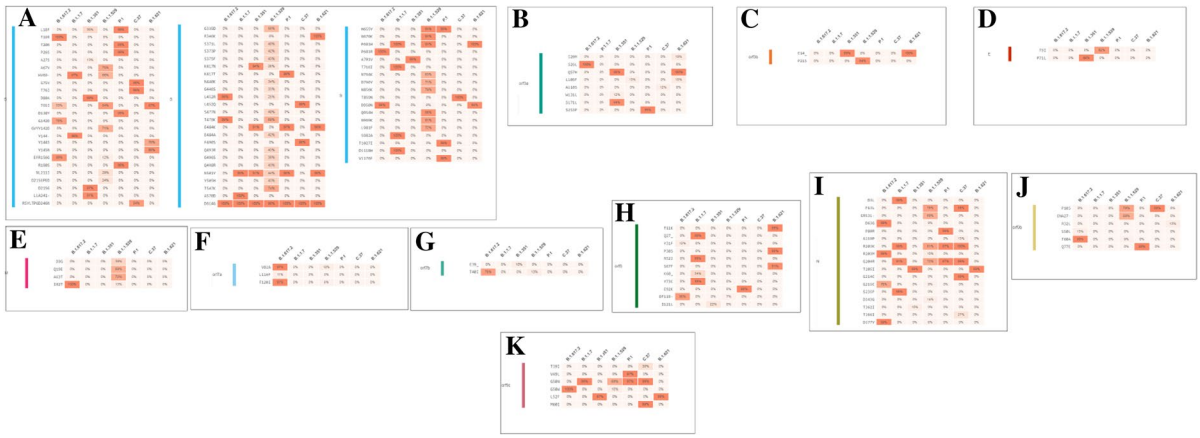

Fig. 8 Amino acid (AA) variants in the structural proteins of Omicron along with other VOCs and VOIs. (**A**) AA variants in S-glycoprotein, (**B**) AA variants in ORF3a, (**C**) AA variants in ORF3b, (**D**) AA variants in E, (**E**) AA variants in M, (**F**) AA variants in ORF7a, (**G**) AA variants in ORF7b, (**H**) AA variants N, (**I**) AA variants in ORF8b, (**J**) AA variants in ORF9b, (**K**) AA variants in ORF9c. In this part of the study, we have also used the COVID-19 CG server to analyze the amino acid (AA) variants of structural proteins of Omicron along with other VOCs and VOIs [48]. The server used the data from the GISAID ingestion pipeline, which is an open source data [48]

with 100% mutational frequency was found in the M protein of the Delta variant.

In ORF7a, one AA variant (V28A) with meager (10%) mutational frequency in the Omicron variant cannot be considered as an AA variant (Fig. 8F). However, two AA variants (V28A and T120I) were noted, each with 97% mutational frequencies in both cases in the Delta variant.

One AA variant (V28A) with meager (13%) mutational frequency in the Omicron variant in ORF7b cannot be considered an AA variant (Fig. 8G). However, one AA variant (T40I) was noted, with a 76% mutational frequency in the Delta variant.

In ORF8, one AA variant (DF119) with a deficient (7%) mutational frequency in the Omicron variant could not be considered an AA variant (Fig. 8H). However, we found that the same AA variant (DF119) had a significant mutational frequency (86%) in the Delta variant.

Four AA variants (P13L, ERS31, R203K, and G204R) with 78%, 69%, 81%, and 72% mutational frequencies, respectively, were found in Omicron in the N protein (Fig. 8I). Simultaneously, four AA variants (D63G, R203M, G215C, and D377Y) with 99%, 99%, 75%, 99% mutational frequencies respectively were found in the N protein of the Delta variant.

In ORF9b, two AA variants (P10S, ENA27-) with 78% and 69% mutational frequencies were found in Omicron (Fig. 8J). However, we found 99% mutational frequency in one AA variant (T60A) in the Delta variant and one AA variant (Q77E) in the Gamma variant.

Finally, we found one AA variant (G50N) with 69% mutational frequency Omicron in orf9c (Fig. 8K). However, we found 100% mutational frequency in one AA variant (G50W) in the Delta variant. We also found 99% mutational frequency in one AA variant (G50N) in Alpha, two AA variants (G50N, M60I) in Lambda, and one AA variant (L52F) in Mu.

Nikolaidis et al. analyzed the amino acid substitutions (AAS) and found a high rate in the spike of the Omicron [60]. Zhang et al. also evaluated AA mutations in different circulating VOCs, including Omicron. They also illustrated cross-species tropism in cells expressing 18 ACE2 molecules. This study may help to forecast the spread of mutations [61].

Heat map-like structure of mutation prevalence with > 75% mutational frequency in Omicron and comparison with the mutations with other VOCs and VOIs

Scientists have evaluated and illustrated the SARS-CoV-2 mutations, their occurrence frequencies, and their circumstances [62–64]. This will assist the researchers in understanding the role of this variant in epidemiology.

We analyzed the mutation prevalence of Omicron, compared the mutations with other VOCs and VOIs, and represented them using a heat map. The heat map shows eight mutations with > 90% identity (K856R, S2083I, DEL2084/2084, A2710T, T3255I, P3395H, DEL3674/3676, and I3758V) in ORF1a in Omicron (Fig. 9A). Similarly, the heat map shows one mutation with > 90% (P314L) and one with > 75% (I1566V) mutation prevalence in ORF1b of Omicron (Fig. 9B). Delta had three mutations (P314L, G662S, P1000L) with > 90% and one mutation (A1918V) with > 80% mutation prevalence. Interestingly, the heat map showed 29 mutations with a > 75% mutation prevalence in the S protein (Fig. 9C). No mutations with > 75% mutation prevalence were found in ORF3a in Omicron (Fig. 9D). Simultaneously, we found some mutations (Delta with S26L, Beta with Q57H, and S171L, Gamma with S253P, Mu with Q57H, and Del 256/257) with > 75% mutation prevalence in ORF3a with other VOCs and VOIs. We found one mutation (T9I) with a > 75% mutation prevalence in Omicron in the E protein and compared it with other VOCs and VOIs (Fig. 9E). We found one mutation (P71L) with a > 75% mutation prevalence in Beta. The heat map of the M protein showed that Omicron had three mutations (D3G, Q19E, and A63T) (Fig. 10A). ORF7a, with a > 75% mutation prevalence, was noted in Omicron. However, Delta had two mutation prevalence rates of > 75% (V82A and T120I) (Fig. 10B). ORF7b, with no mutation with > 75% prevalence, was noted in Omicron. However, Delta had a prevalence of > 75%, corresponding to T40I (Fig. 10C). We observed that the prevalence of S84L was > 75% for all ORF8 variants. The only mutation prevalence observed for Omicron with > 75% (Fig. 10D). Finally, we noted that the prevalence of the four Omicron mutations, P13L, DEL31/33, R203K, G204R was > 75% in N (Fig. 10E). We also noted four mutations with

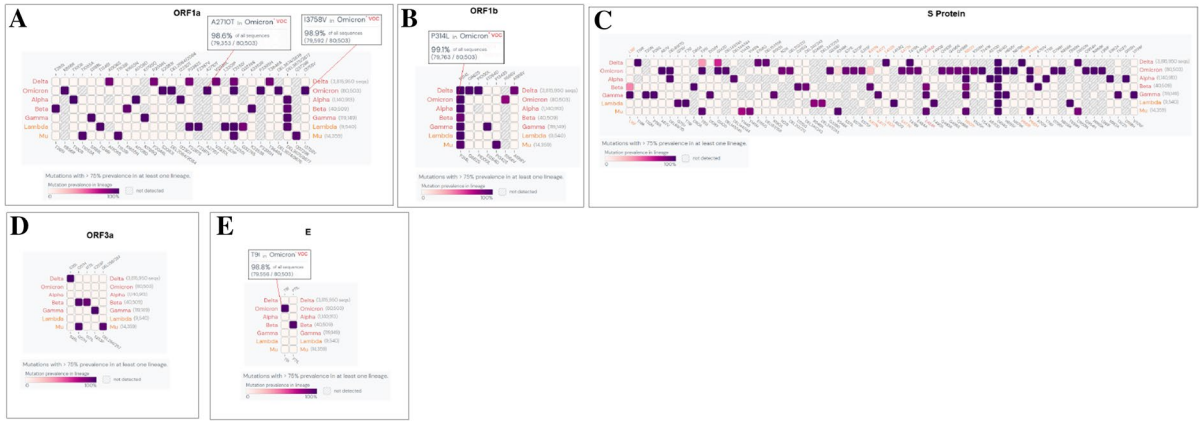

Fig. 9 The heat map-like representation shows the high mutation prevalence (> 75% mutational frequency) of Omicron and other VOCs and VOIs in ORF1a, ORF1b, S-glycoprotein, ORF3a, E. (**A**) Heat map of ORF1a. (**B**) Heat map of ORF1b. (**C**) Heat map of S-glycoprotein. (**D**) Heat map of ORF3a. (**E**) Heat map of E. Here, we have used outbreak.info [51] to provide the heat map like representation of high mutation (AA mutation) prevalence (> 75% mutational frequency) of Omicron and other VOCs and VOIs of different parts of the genome. The server used GISAID API data and integrated the EpiData pipeline [65] from Johns Hopkins University if needed and finally represented through a graphical interface

a prevalence of > 75% in Delta, Alpha, and Lambda. Characteristic mutations for Omicron and comparison with the mutations of other VOCs and VOIs were noted as deletions or nonsynonymous substitutions, which have taken place in > 75% of sequences within those variants. In this study, we measured the mutations of Omicron with > 75%. Simultaneously, this study assisted in understanding the mutations of VOCs and VOIs with > 75% (Alpha, Beta, Gamma, Delta, Lambda, and Mu). From the heat map, we found that AA variants with high mutation prevalence showed eight mutations with > 90% prevalence in ORF1a and 29 mutations with > 75% prevalence in the S-glycoprotein of Omicron. Our study is significant in this regard.

Scatter plot for cluster evaluation of Omicron and other VOCs and VOIs

Cluster analysis was performed, and a scatter plot was generated for all current VOCs and VOIs, in conjunction with the Omicron variant. The scatter plot shows the prevalence of all VOCs and VOIs with Omicron and indicates the origin and distribution of all current VOCs and VOIs. A scatter plot with linear regression was developed using the current circulating VOCs and VOIs (Fig. 11A). The model informs us that all the sample values were placed on both sides of the regression line. The figure shows a strong, positive, and linear scatter plot. Simultaneously, the scatter plot of the Omicron variant shows the prevalence of all samples on the upper side of the regression line (Fig. 11B).

Similarly, the scatter plot of the Delta variant shows the prevalence of all sample points on both sides of the regression line of the plot (Fig. 12A). The scatter plot of the Alpha variant shows the prevalence of all sample points above the regression line. All sample points were in the middle position of the regression line (Fig. 12B). Similarly, the scatter plot of the Beta variant shows the prevalence of all sample points below the regression line. However, a few sample points were placed above the regression line, and all sample points were placed middle in the position of the regression line (Fig. 12C).

Similarly, the scatter plot of the Gamma variant shows the prevalence of all sample points in the upper region of the regression line. Most sample points were above the regression line. However, a few sample points are found below the plot's regression line (Fig. 12D).

Similarly, the scatter plot of the Lambda variant shows the prevalence of all sample points in the upper region of the regression line. Most of the sample points were below the regression line, and however, very few sample points were observed above the regression line (Fig. 12E).

Fig. 10 The heat map-like representation shows the high mutation prevalence (> 75% mutational frequency) of Omicron and other VOCs and VOIs in M, ORF7a, ORF7b, ORF8, N. (**A**) Heat map of M. (**B**) Heat map of ORF7a. (**C**) Heat map of ORF7b. (**D**) Heat map of ORF8. (**E**) Heat map of N. Here, we have also used outbreak.info [51] to provide the heat map-like representation of high mutation (AA mutation) prevalence (> 75% mutational frequency) of Omicron and other VOCs and VOIs. The server used GISAID API data and integrated the EpiData pipeline [65] from Johns Hopkins University if needed and finally represented through a graphical interface

Finally, we developed a scatter plot for the Mu variants. The figure shows the prevalence of all sample points in the upper region of the regression line of the plot. Most of the sample points were below the regression line. However, few sample points were found above the regression line (Fig. 12F). The scatter plots for the Lambda and Mu variants are quite similar. However, it was observed that the Mu variant sample points were densely placed (Fig. 12E, F).

Prevalence of mutations in the neutralizing antibody (NAb) binding site in Omicron and other VOCs and VOIs

Mutations in the nAb binding site or close to the nAb binding site of the S-glycoprotein of the Omicron variant have been noted. We analyzed the mutations in the nAb binding site from an extensive survey of the typical nAb (type-1 to type-4) interaction with the S-glycoprotein and found mutations in the nAb binding site or close to the nAb binding site of the S-glycoprotein. The most emerging mutations in the antibody interaction area were located within the RBD region (Fig. 13A).

Similarly, mutations in the nAb binding site or close to the nAb binding site of the S-glycoprotein of the other VOCs are also illustrated (Fig. 13B). We also recorded mutations in the nAb binding site or close to the nAb binding site of the S-glycoprotein of the other VOIs (Fig. 13C). We performed a comparative analysis of mutations in the nAb binding site of all VOCs and VOIs to assess the emerging mutations

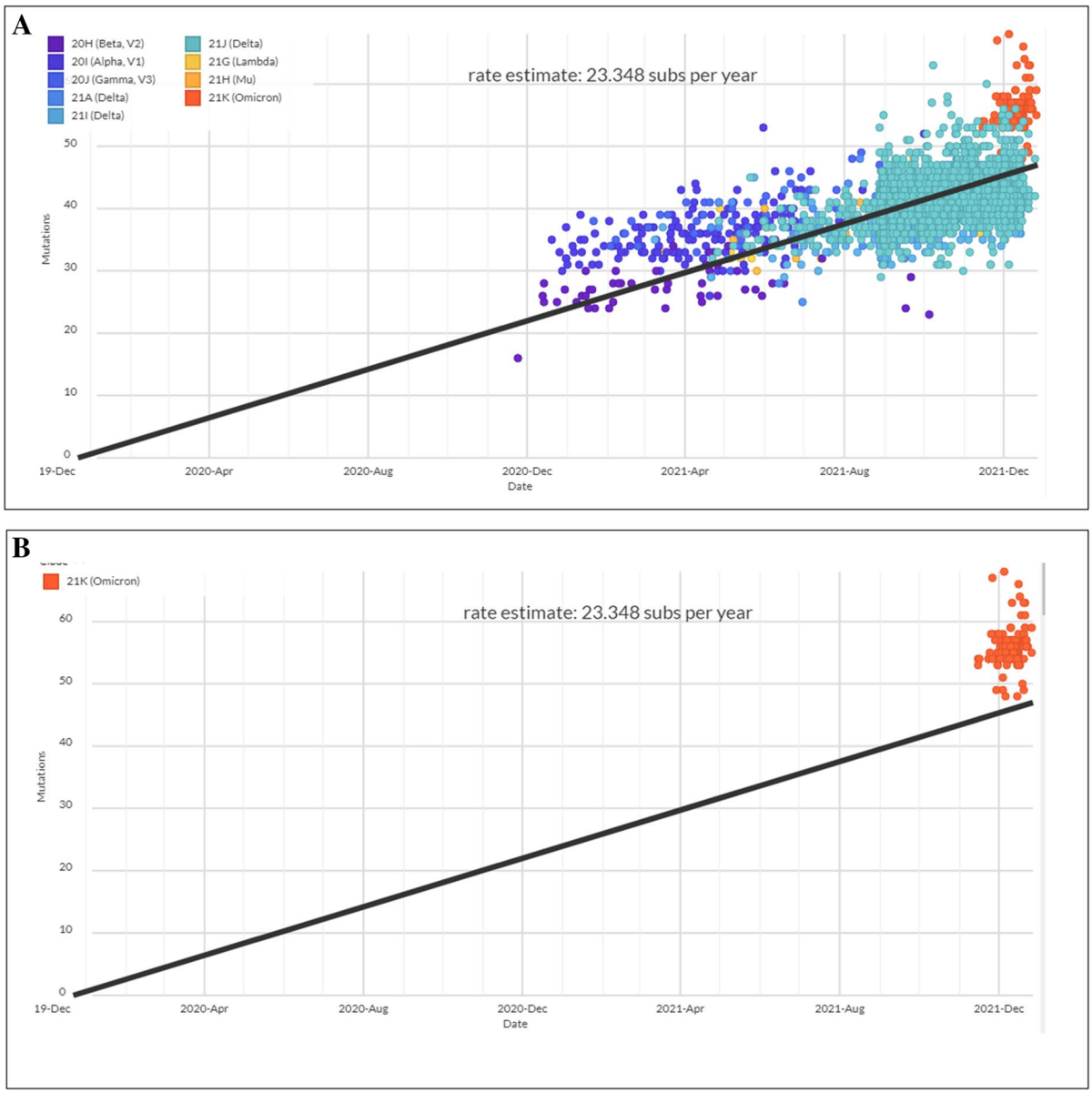

Fig. 11 Scatter plot for cluster evaluation of Omicron and all VOCs and VOIs. (**A**) Scatter plot for cluster evaluation of all VOCs and VOIs. (**B**) Scatter plot for cluster evaluation of Omicron. The scatter plot was developed for Omicron and all VOCs and VOIs using the Nextstrain server [49, 50]. The server used the GISAID data

in the nAb binding site of the S-glycoprotein, and illustrated all crucial mutations in the nAb binding area (Table 4).

Zhang et al. illustrated mutations in 11 VOCs and VOIs, including Omicron, and their effect on the nAb binding site. They concluded from their study that mutations near AA 439–448 and AA484 might cause resistance to neutralization [61]. Cui et al. performed an experimental study and developed the Omicron pseudo-virus, attempted to correlate immunogenic areas with high mutation frequencies, and correlated them with properties such as immune escape and infectivity. They identified the ten most critical immunogenic residues. Among them, the three AA substitution residues were Y505H,

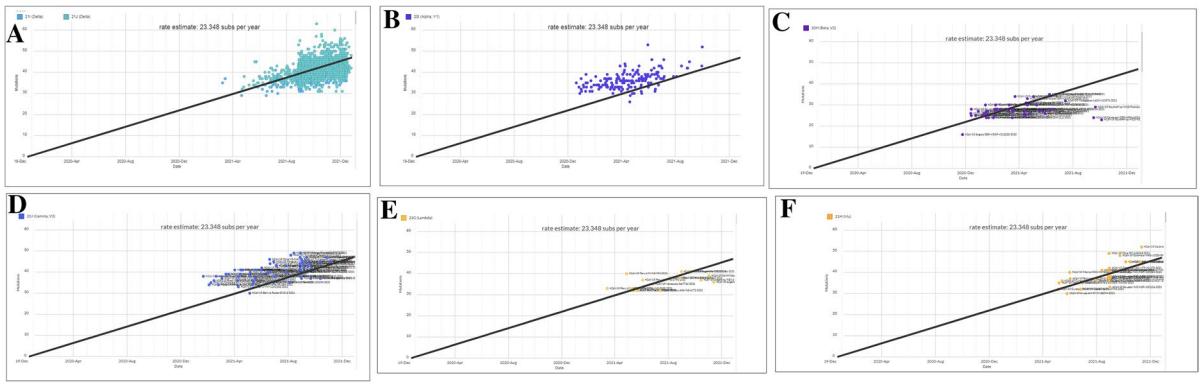

Fig. 12 Scatter plot for cluster evaluation for VOCs and VOIs. (**A**) Scatter plot for cluster evaluation of Delta. (**B**) Scatter plot for cluster evaluation of Alpha. (**C**) Scatter plot for cluster evaluation of Beta. (**D**) Scatter plot for cluster evaluation of Gamma. (**E**) Scatter plot for cluster evaluation of Lambda. (**F**) Scatter plot for cluster evaluation of mu. The scatter plot was developed for VOCs and VOIs using the Nextstrain server [49, 50]. The server used the GISAID data

E484A/K, and Q493R. They have noted some other significant residues, including F456, N487, Y449, Y489, and F486 [66]. Similarly, in another experimental study, Planas et al. illustrated 32 spike mutations, mostly in NTD, which may augment viral fitness and antibody escape [67]. In the present study, we also depicted mutations nAb binding site or close to the nAb binding site of the S-glycoprotein, which may increase viral fitness and nAb escape.

Risk analysis of antibody-binding to significant antibody-binding mutations in the RBD in the S-glycoprotein

We performed an analysis to understand the risk level of mutations in four positions and found that three AA residues are essential for interactions with the antibody. In this study, we analyzed three positions for mutations (L452, F490, and P681) and a significant mutation (D614G).

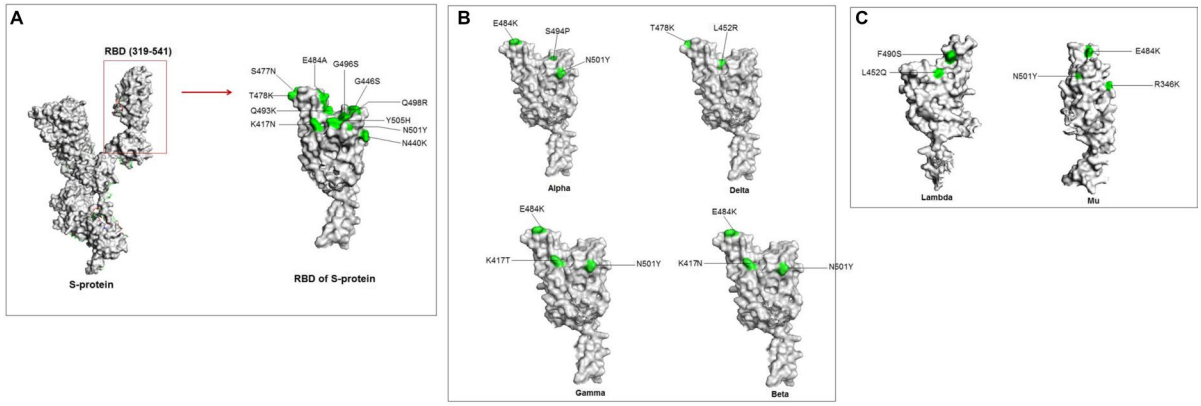

Fig. 13 The figure shows the developed 3D model of S-glycoprotein and the emerging mutations. The major mutations are located within the RBD region, which might involve antibodies interaction area. (**A**) RBD mutations in Omicron located in antibody interaction region. (**B**) RBD mutations in VOIs located in antibody interaction region. (**C**) RBD mutations in VOIs located in the antibody interaction region. The 3D model of S-glycoprotein using PyMOL software and the emerging mutations for antibody interaction was depicted for the Omicron variant, other VOC, and VOI in the 3D model [46, 47]. For a 3D model generation, we used some PDB files (PDB ID: 6VXX)

Table 4 Emerging mutations in antibodies interaction area within RBD region of SARS-CoV-2 VOCs and VOIs including Omicron variant

Sl no	Variants name (WHO label)	SARS-CoV-2 lineages	Mutations in S-protein (RBD region)	Remarks
1	Omicron	B.1.1.529	K417N, N440K, G446S, S477N, T478K, E484A, Q493K, G496S, Q498R, N501Y, Y505H	Comparative analysis from all present VOCs and VOIs noted the following mutations in Ab interaction within the RBD region: K417N, N440K, G446S, S477N, T478K, E484A, Q493K, G496S, Q498R, N501Y, Y505H, S494P, L452R, T478K, K417T, L452Q, F490S, R346K
2	Alpha	B.1.1.7	E484K, S494P, N501Y	
3	Delta	B.1.617.2	L452R, T478K	
4	Gamma	P.1	K417T, E484K, N501Y	
5	Beta	B.1.351	K417N, E484K, N501Y	
6	Lambda	C.37	L452Q, F490S	
7	Mu	B.1.621	R346K, E484K, N501Y	

The mutation risk of the L452 location was analyzed, and the risk level of 19 different types of mutational variants at a particular site (L452) is illustrated (Fig. 14A). The L452R mutation has a destabilizing effect on the interactions of S-glycoprotein targeting antibodies. Variants of the mutation have also been reported (Fig. S1A). The count for this variant of the L452R mutation is 1657075, and the first variant (L452R) was identified in the USA.

We analyzed the mutation risk at the F490 position, and 19 different types of mutations in different variants at this position (F490) were observed (Fig. 14B). The F490S mutation was found to have a destabilizing effect on antibody interactions. Variants of this mutation have also been reported (Fig. S1B). The count for this variant of the F490S mutation was 13,311, and the first variant (F490S) was identified in Canada.

We analyzed the mutation risk at the P681 position. Similarly, previous mutations and the 19 different types of mutations in different variants (P681) were explained (Fig. 14C). In the P681 mutation, it has been noted that the mutations do not have any destabilizing effect on the antibody interactions. Variants of this mutation have also been reported (Fig. S1C). The count for this variant of the P681H

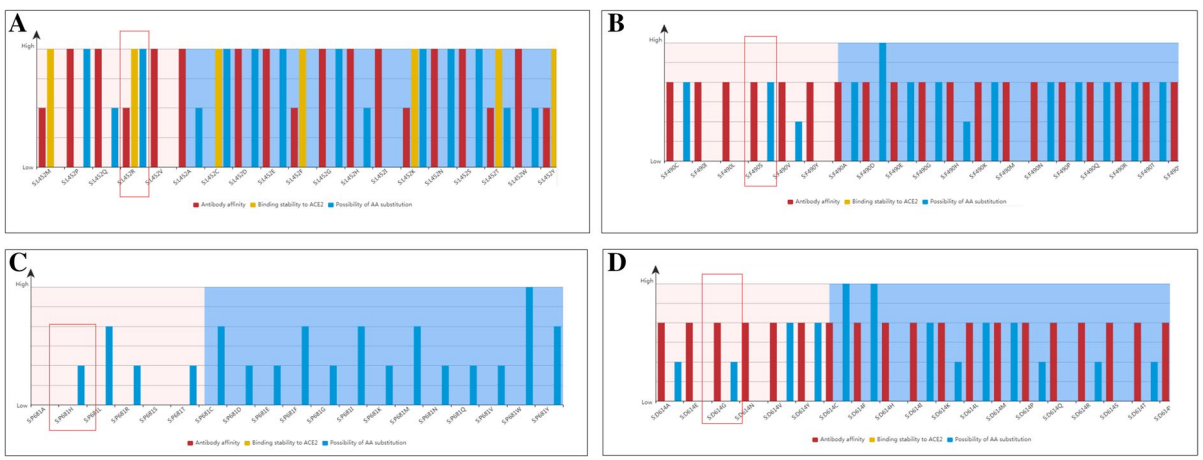

Fig. 14 Risk analysis of antibody-binding to significant some antibody-binding mutations and its other variants. (**A**) Risk analysis of antibody-binding to L452 region and L452R mutation. (**B**) Risk analysis of antibody-binding to F490 region and F490S mutation. (**C**) Risk analysis of antibody-binding to P681 region and P681H mutation. (**D**) Risk analysis of antibody-binding to D614 region and D614G mutation. We used the VarEPS server to evaluate the risk analysis of antibody-binding of some antibody-binding mutations [52]. The server used the GISAID data and data from other resources such as CDC China, CDC, USA, WHO

mutation was 130,2751, and the first mutation (P681H) was identified in Nigeria.

Finally, 19 different types of mutations in different variants of D614G are shown (Fig. 14D). The D614G mutation has a destabilizing effect on the antibody interactions. Variants of the mutation have also been reported (Fig. S1D). The count for this variant of the D614G mutation was 4,105,183, and the first variant (D614G) was reported in Germany.

Molecular and mutational properties of some significant RBD mutations in Omicron

Mutations in the RBD region may play a role in antibody, immune, or vaccine escape. In this part of the analysis, we evaluated some RBD mutations' molecular and mutational properties in the Omicron variants: G339D, S371L, N440K, G446S, T478K, and Q498R. The study illustrated several molecular and mutational parameters such as delta delta G (DDG) or ΔΔG, interatomic interactions in the wild-type and mutant-type residues, and fluctuation and deformation analysis of those mutations. We also analyzed the fluctuation of the wild-type and mutant-type residues, atomic fluctuation in the wild-type and mutant-type of the S-glycoprotein, and deformation energies in the wild-type and mutant-type of the S-glycoprotein in respect of these mutations.

We assessed the molecular and mutational properties of G339D. The molecular and mutational parameters (ΔΔG, interatomic interactions, and fluctuation and deformation analysis) of G339D are illustrated in Fig. 15A. Here, the analysis indicated that the outcome of ΔΔG was 0.019 kcal/mol (stabilizing). The NMA-based predictions showed that ΔΔG ENCoM was − 0.027 kcal/mol (destabilizing). Other structure-based calculations showed that ΔΔG mCSM was − 0.691 kcal/mol (destabilizing), ΔΔG SDM was 0.110 kcal/mol (stabilizing), and ΔΔG DUET was − 0.400 kcal/mol (destabilizing). The ΔΔSVib ENCoM (minute vibrational entropy energy between wild-type and mutant-type) was 0.033 kcal/mol^{-1} K^{-1}. This model indicates that the mutation increases molecular flexibility, as shown in Fig. 15B. Here, the wild-type and mutant-type residues are colored light green. The model informed the neighboring residues linked to the interaction interface. Figure S2A shows the fluctuation of the wild-type and mutant-type residues. Visual analysis shows atomic fluctuation in the 3D model of the S-glycoprotein, both in the wild-type and mutant-type (Fig. S2B). Simultaneously, the study included a visual analysis of deformation energies to show the amount of local flexibility of the 3D model of both the wild-type and mutant-type S-glycoproteins (Fig. S2C).

The molecular and mutational properties of S371L were also evaluated. Here, we illustrated the molecular and mutational factors in G339D (Fig. 16A). The analysis indicated that the outcome of ΔΔG was 0.127 kcal/mol (stabilizing). The NMA-based predictions showed that ΔΔG ENCoM was 0.030 kcal/mol (destabilizing). Other structure-based calculations showed that ΔΔG mCSM was − 0.394 kcal/mol (destabilizing), ΔΔG SDM was 1.280 kcal/mol (stabilizing), and ΔΔG DUET was 0.080 kcal/mol (stabilizing). The evaluation of (ΔΔSVib ENCoM) change

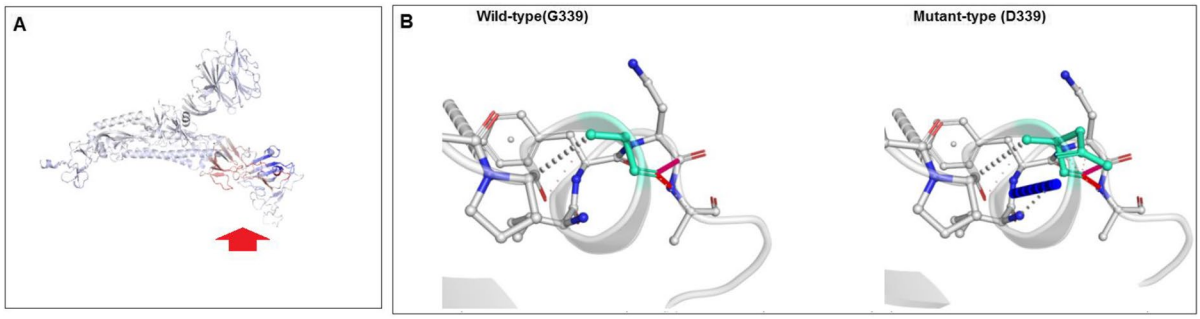

Fig. 15 Mapped molecular and mutational properties of G339D. (**A**) Prediction of vibrational Entropy Energy of G339D with a visual representation. (**B**) Prediction of interatomic interactions of wild type to mutant type G339D mutation. In this study, we used the DynaMut server to evaluate the molecular and mutational properties of G339D [53]. For the analysis, we used a model PDB file (PDB ID: 7QO7)

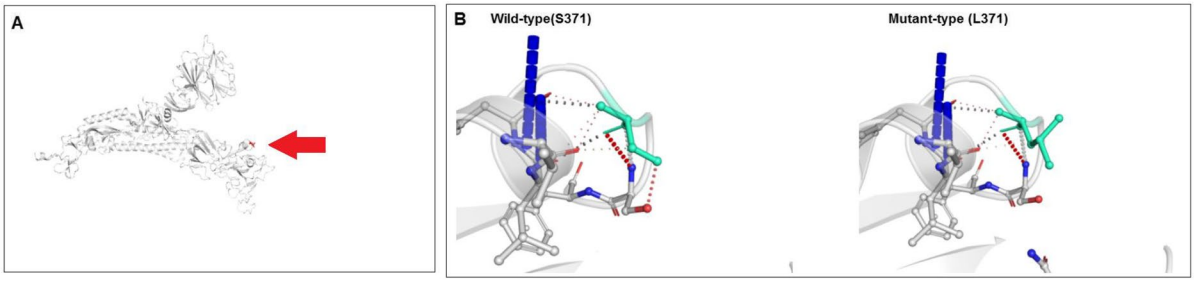

Fig. 16 Evaluated molecular and mutational properties of S371L. (**A**) Calculation of vibrational Entropy Energy of S371L with a visual representation. (**B**) Prediction of interatomic interactions of wild type to mutant type S371L mutation. For this evaluation, the DynaMut server was used to evaluate the molecular and mutational properties of S371L [53]. For the analysis, we used a model PDB file (PDB ID: 7QO7)

between wild-type and mutant-type was − 0.037 kcal/mol^{-1} K^{-1}. The mutational landscape indicated that the mutation decreased molecular flexibility. The molecular contacts between the inter-atoms are illustrated in Fig. 16B. The light green residues indicate the wild-type and mutant-type AA residues in this study. The developed model indicated that adjoining residues were related to the interaction interface. Figure S3A shows the fluctuation of the wild-type and mutant-type residues. Visual analysis shows atomic fluctuation in the 3D model of the S-glycoprotein for both the wild-type and mutant-type (Fig. S3B). We evaluated the visual analysis of deformation energies, showing the quantity of local flexibility of the 3D model of both the wild-type and mutant-type S-glycoprotein (Fig. S3C).

This study analyzed parameters such as ΔΔG, interatomic interactions, and fluctuation and deformation to understand the molecular and mutational properties of the N440K mutation. The results of ΔΔG analysis of N440K mutation are shown in Fig. 17A. Here, the analysis indicated that the outcome of ΔΔG was 0.064 kcal/mol (stabilizing). The NMA-based predictions showed that ΔΔG ENCoM was 0.045 kcal/mol (destabilizing). Other structure-based calculations showed that ΔΔG mCSM was 0.243 kcal/mol (stabilizing), ΔΔG SDM was 0.780 kcal/mol (stabilizing), and ΔΔG DUET was 0.876 kcal/mol (stabilizing). The evaluation of minute vibrational entropy energy between the wild-type and mutant-type (ΔΔSVib ENCoM) indicated as − 0.057 kcal mol^{-1} K^{-1}. The result of the model predicts that the mutation decreases molecular flexibility. The interactions between the inter-atoms are shown in Fig. 17B. The wild-type and mutant-type residues are marked in light green. The model revealed the adjacent residues involved in the interaction. Figure S4A illustrates the fluctuation of wild-type and mutant-type residues. Visual analysis showed atomic fluctuation in the 3D model of the

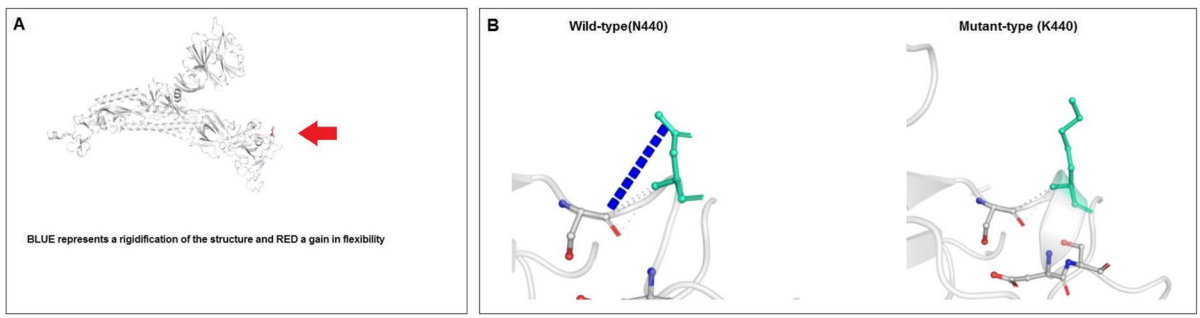

Fig. 17 Analyzed result of molecular and mutational properties of N440K. (**A**) Computation of vibrational Entropy Energy of N440K and is represented through a pictorial view. (**B**) Prediction of interatomic Interactions of wild type to mutant type N440K mutation. In this study, we used the DynaMut server to assess the molecular and mutational properties of N440K [53]. For the analysis, we used a model PDB file (PDB ID: 7QO7)

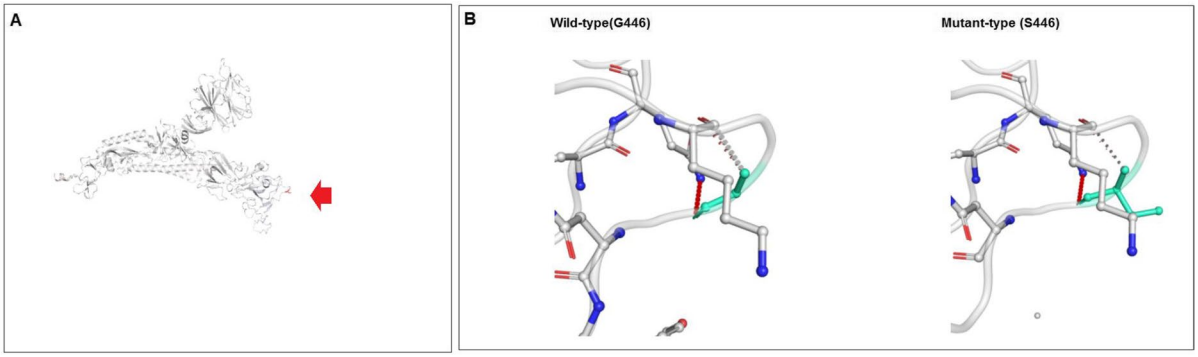

Fig. 18 Evaluated outcome of the molecular and mutational properties of G446S. (**A**) Calculated vibrational Entropy Energy of G446S and its pictorial representation. (**B**) Illustrated interatomic interactions of wild type to mutant type G446S mutation. For this analysis, the DynaMut server was used to evaluate the molecular and mutational properties of S371L [52]. For the analysis, we used a model PDB file (PDB ID: 7QO7)

S-glycoprotein, both in the wild-type and mutant-type (Fig. S4B). Simultaneously, the study evaluated the visual analysis of deformation energies to show the amount of local flexibility of the 3D model of both the wild-type and mutant-type S-glycoproteins (Fig. S4C).

This study analyzed several parameters to evaluate the molecular and mutational features of the G446S mutation. Figure 18A shows the results of ΔΔG analysis of the G446S mutation. In this investigation, the effect of ΔΔG was recorded as − 0.501 kcal/mol (destabilizing). The NMA-based calculation showed that ΔΔG ENCoM was − 0.283 kcal/mol (destabilizing). Additional structure-based computations indicated that ΔΔG mCSM was − 0.593 kcal/mol (destabilizing), ΔΔG SDM was − 0.680 kcal/mol (destabilizing), and ΔΔG DUET was − 0.366 kcal/mol (destabilizing). We evaluated minute vibrational entropy energy change between wild-type and mutant-type, which shows ΔΔSVib ENCoM: − 0.353 kcal/mol^{-1} K^{-1}. The results of the model indicated a mutational landscape augmentation of molecular flexibility. The inter-atomics interactions are shown in Fig. 18B. The model depicts the wild-type and mutant-type residues as light green and shows the nearby residues involved in the interface. Figure S5A shows the fluctuation of the wild-type and mutant-type residues. Visual analysis showed that the atomic fluctuation in the 3D model indicated both in the wild-type and mutant-type S-glycoprotein (Fig. S5B). We visually analyzed the deformation energies to show the amount of local flexibility through the 3D model of wild-type and mutant-type S-glycoproteins (Fig. S5C).

We recorded the results of ΔΔG for the T478K mutation in Fig. 19A. In the computation, the effect

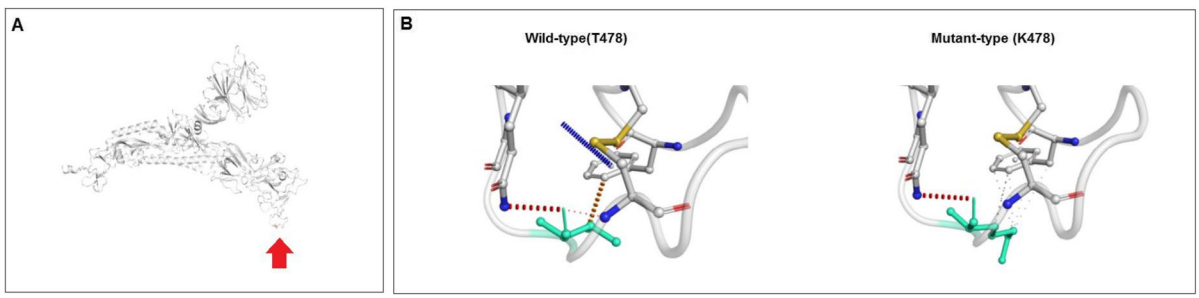

Fig. 19 Analyzed result of the molecular and mutational properties of T478K. (**A**) Calculated vibrational Entropy Energy of T478K and its visual representation. (**B**) Illustrated of interatomic interactions of wild type to mutant type T478K mutation. We have used the DynaMut server in this study to explain the molecular and mutational properties of N440K [53]. For the analysis, we used a model PDB file (PDB ID: 7QO7)

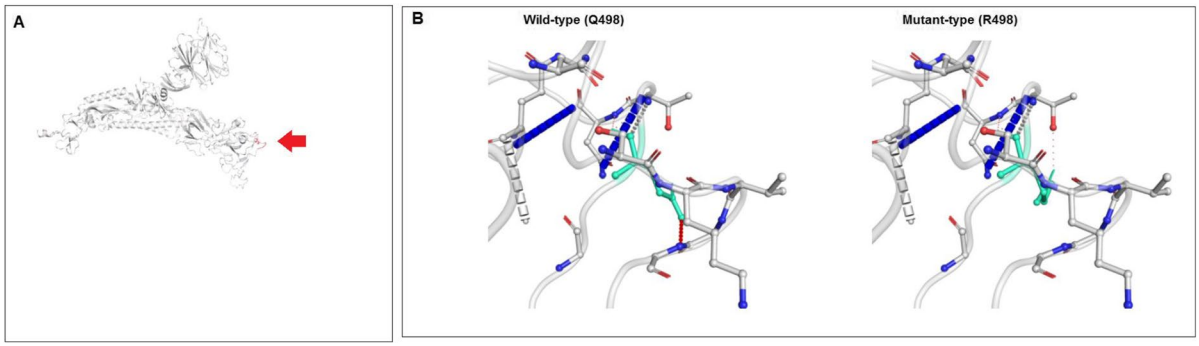

Fig. 20 Representation of the molecular and mutational properties of Q498R. (**A**) Calculated vibrational Entropy Energy of Q498R and its visual representation. (**B**) Illustrated interatomic interactions of wild type to mutant type Q498R mutation. We have used the DynaMut server in this study to elucidate the molecular and mutational properties of Q498R [53]. For the analysis, we used a model PDB file (PDB ID: 7QO7)

of ΔΔG was recoded as 1.009 kcal/mol (stabilizing). The NMA-based estimation showed that ΔΔG ENCoM was 0.181 kcal/mol (destabilizing). Further structure-based analysis indicated three ΔΔG-based parameters ΔΔG mCSM, − 0.695 kcal/mol (destabilizing), ΔΔG SDM (− 0.070 kcal/mol; destabilizing), and ΔΔG DUET (− 0.366 kcal/mol (destabilizing). The ΔΔSVib ENCoM change between wild-type and mutant-type was found to be − 0.227 kcal/mol^{-1} K^{-1}. The result of the model informed us about mutational flexibility (decreased molecular flexibility). The interatom correlations are shown in Fig. 19B. The developed model of the wild-type and mutant-type residue indicated in light green, which informs us that adjunct residues are involved in the interaction interface. The fluctuation of the wild-type and mutant-type residues are shown in Figure S6A. Visual analysis revealed atomic fluctuation of the wild-type and mutant-type of the S-glycoprotein (Fig. S6B). We evaluated the visual analysis of deformation energies to show the amount of local flexibility through a model that provides a pictorial view of both the wild-type and mutant-type S-glycoprotein (Fig. S6C).

Finally, the mutational features and molecular properties of the Q498R mutation were assessed. We observed the properties of ΔΔG and its effect on the mutant type of the Q498R mutation, as illustrated in Fig. 20A. This analysis recorded the consequence of ΔΔG due to the Q498R mutation as − 0.163 kcal/mol (destabilizing). The computation of NMA-related predictions showed that ΔΔG ENCoM was − 0.289 kcal/mol (destabilizing). Additionally, three structure-based analyses indicated ΔΔG-related features of the mutation. The results were as follows: ΔΔG mCSM was 0.283 kcal/mol (stabilizing), ΔΔG SDM was 0.550 kcal/mol (stabilizing), and ΔΔG DUET was 0.519 kcal/mol (stabilizing). The ΔΔSVib ENCoM, calculated as 0.361 kcal/mol^{-1} K^{-1}, was noted as increased the molecular flexibility of the S-glycoprotein. We depicted the inter-atom configurations of the mutational landscape of the wild and mutant varieties of Q498R, which is illustrated in Fig. 20B. A model was generated for the wild-type and mutant-type residues, illustrating both residues as light green. The model showed that the residues associated with that particular position were also associated with the interaction interface. Figure S7A shows the fluctuation of the wild-type and mutant-type residues. Furthermore, visual analysis of atomic fluctuation in the mutant residue informed us about the atomic fluctuation of the wild-type and mutant-type spike-glycoproteins (Fig. S7B). Moreover, the experiment illustrated the deformation energies of the visual analysis and provide information on the quantity of local flexibility using a bioinformatics model. The model shows the pictographic view of both the wild-type and mutant-type spike-glycoprotein (Fig. S7C).

We have comprehensively analyzed the properties of 28 mutations, and other researchers have tried to analyze other mutations using a similar method [68]. However, our comprehensive study has tried to analyze the 28 mutations along with RBD mutations and concluded how RBD mutations affect receptor

binding of Omicron. Finally, we tried to explain how RBD mutations might affect infectivity.

Comparative analysis of delta-delta G (DDG) or ΔΔG of analyzed mutations in the S-glycoprotein

We performed a comprehensive and comparative analysis of ΔΔG for 28 significant mutations, including K417N, S477N, T478K, D796Y, G196D, G446S, E484A, T95I, D614G, H655Y, Q493K, G496S, N501Y, Y505H, N969K, A67V, L981F, N440K, N856K, Q498R, S371L, G339D, L212I, S375F, S373P, N764K, T547K, and Q954H. The ΔΔG values of the 28 analyzed mutations are shown in Table 5. In this study, we performed several cooperative analyses, including ΔΔG ENCoM, ΔΔG, ΔΔG mCSM, ΔΔG DUET, ΔΔG SDM, and ΔΔSVib ENCoM. The NMA-based prediction of ΔΔG ENCoM analysis showed that the K417N mutation had shown a minimum value with the destabilizing result (−0.677 kcal/mol), and the G196D mutation had a maximum value with a stabilizing result (0.897 kcal/mol). ΔΔG prediction showed that the K417N mutation had a minimum value with a destabilizing impact (−0.932 kcal/mol) and the Q954H mutation had a maximum value with a stabilizing effect (0.969 kcal/mol). Evaluation of Δ vibrational entropy energy between wild-type and mutant ($\Delta\Delta S_{Vib}$ ENCoM) showed that the G196D mutation had a minimum value of −1.121 kcal/mol^{-1} K^{-1}. Similarly, the K417N mutation had a maximum value of 0.846 kcal/mol^{-1} K^{-1}.

Cui et al. reported a stable Omicron spike that helps to maintain an active conformation, which plays a significant role in receptor recognition [66]. Some mutations were observed with increased flexibility which may also help in receptor interactions and, thus, improve viral fitness. Therefore, our predicted mutations with stabilizing properties in the S-glycoprotein, particularly RBD mutation, play a significant role in receptor recognition, increasing infectivity, and improving viral fitness.

Discussion

The Omicron variant has been spreading rapidly in several countries worldwide. Omicron is an immensely mutated emerging variant that is proving to be a challenge to researchers [25, 26]. This variant has the largest number of mutations among all other VOCs and VOIs of SARS-CoV-2, and researchers have described this variant as a rare collection of mutations [69]. More than 50 mutations have been identified in the genome. Researchers have noted approximately 32 in the spike protein [20, 25–27]. Therefore, it is essential to understand the mutational landscape of the Omicron variant and compare the landscape of mutations with other emerging variants. This study attempted to understand the mutational landscape of the Omicron variant and compared all mutational frequencies of SNVs throughout the genome with those of other emerging variants. We evaluated the AA variants in the Omicron variant and compared them with those in the present VOCs and VOIs. This study found that the D614G AA variant in the S-glycoprotein was present in all VOCs and VOIs at a high frequency (98–100%). Our in silico analysis corroborates the previous finding about the high frequency of D614G mutation in Omicron and other VOI/VOC [31, 32, 63]. Analysis of AA variants of the non-structural protein revealed that P323L in nsp12 was also observed in all VOCs and VOIs with high frequency (97–100%). We illustrated the AA variants using a heat map of mutation prevalence with > 75% mutational frequency of Omicron and compared those mutations with that of other VOCs and VOIs. The heat map helps identify mutations with a high mutational frequency. This study showed eight mutations with > 90% in ORF1a and 29 in S-glycoprotein, with > 75% mutation prevalence in Omicron. Several other studies have attempted to illustrate mutations in different regions of the Omicron. Lupala et al. elucidated the interaction between the RBD region of Omicron and the hACE2 receptor to understand its binding affinity. In this study, they developed a model of a mutated RBD region and an interaction model between the RBD region of Omicron and the hACE2 receptor. Finally, MDS (molecular dynamics simulations) were performed to understand the RBD-hACE2 interaction pattern [70]. In our study, we analyzed 28 mutations and observed that among RBD mutations, G339D, S371L, N440K, and T478K mutations are stabilizing, and G446S and Q498R are destabilizing mutations. At the same time, G339D, G446S, and Q498R mutations have increased molecular flexibility. Cumulative effects of the properties

Table 5 Comparative analysis of delta delta G (DDG) or ΔΔG of emerging mutations of S-glycoprotein in Omicron variant

		NMA based prediction	ΔΔG prediction	Other structure-based predictions			Minute vibrational entropy energy change between wild-type and mutant	Remarks
Sl no	Significant mutations of Omicron variant	ΔΔG ENCoM (kcal/mol)	ΔΔG (kcal/mol)	ΔΔG mCSM (kcal/mol)	ΔΔG DUET (kcal/mol)	ΔΔG SDM (kcal/mol)	$\Delta\Delta S_{Vib}$ ENCoM (kcal mol^{-1} K^{-1})	
1	K417N	−0.677, Destabilizing	*−0.932,* Destabilizing	−1.138, Destabilizing	−1.123, Destabilizing	−0.280, Destabilizing	0.846	Increase of molecule flexibility increased
2	S477N	0.064, Destabilizing	*0.628,* Stabilizing	−0.215, Destabilizing	0.235, Stabilizing	0.780, Stabilizing	−0.080	Decrease of molecule flexibility
3	T478K	0.181, Destabilizing	*1.009,* Stabilizing	−0.695, Destabilizing	−0.366, Destabilizing	−0.070, Destabilizing	−0.227	Decrease of molecule flexibility
4	D796Y	−0.052, Destabilizing	*0.146,* Stabilizing	0.387, Stabilizing	0.370, Stabilizing	−0.010, Destabilizing	0.065	Increase of molecule flexibility
5	G196D	0.897, Stabilizing	*0.193,* Stabilizing	−2.071, Destabilizing	−2.248, Destabilizing	−2.160, Destabilizing	−1.121	Decrease of molecule flexibility
6	G446S	−0.283, Destabilizing	−0.501, Destabilizing	−0.593, Destabilizing	−0.366, Destabilizing	−0.680, Destabilizing	0.353	Increase of molecule flexibility
7	E484A	−0.377, Destabilizing	−0.456, Destabilizing	−0.415, Destabilizing	−0.128, Destabilizing	0.320, Stabilizing	0.471	Increase of molecule flexibility
8	T95I	0.320, Destabilizing	1.200, Stabilizing	−0.097, Destabilizing	0.670, Stabilizing	1.910, Stabilizing	−0.400	Decrease of molecule flexibility
9	D614G	−0.134, Destabilizing	0.351, Stabilizing	−0.514, Destabilizing	0.171, Stabilizing	2.510, Stabilizing	0.168	Decrease of molecule flexibility
10	H655Y	0.158, Destabilizing	1.728, Stabilizing	1.302, Stabilizing	1.516, Stabilizing	0.400, Stabilizing	−0.197	Decrease of molecule flexibility
11	Q493K	0.066, Destabilizing	0.470, Stabilizing	0.194, Stabilizing	0.794, Stabilizing	0.580, Stabilizing	−0.082	Decrease of molecule flexibility
12	G496S	−0.014, Destabilizing	−0.097, Destabilizing	−0.763, Destabilizing	−0.614, Destabilizing	−1.010, Destabilizing	0.018	Decrease of molecule flexibility
13	N501Y	−0.094, Destabilizing	−0.203, Destabilizing	−0.457, Destabilizing	−0.471, Destabilizing	0.280, Stabilizing	0.117	Decrease of molecule flexibility
14	Y505H	−0.305, Destabilizing	−0.510, Destabilizing	−0.119, Destabilizing	0.143, Stabilizing	0.380, Stabilizing	0.381	Decrease of molecule flexibility

Table 5 (continued)

		NMA based prediction	ΔΔG prediction	Other structure-based predictions			Minute vibrational entropy energy change between wild-type and mutant	Remarks
15	N969K	−0.381, Destabilizing	0.086, Stabilizing	0.065, Stabilizing	0.184, Stabilizing	−0.500, Destabilizing	0.477	Increase of molecule flexibility
16	A67V	0.520, Stabilizing	0.544, Stabilizing	−0.387, Destabilizing	0.256, Stabilizing	0.950, Stabilizing	−0.650	Decrease of molecule flexibility
17	L981F	0.009, Destabilizing	0.104, Stabilizing	−1.241, Destabilizing	−1.289, Destabilizing	−0.69, Destabilizing	0.012	Increase of molecule flexibility
18	N440K	*0.045,* Destabilizing	0.064, Stabilizing	0.243, Stabilizing	0.876, Stabilizing	0.780, Stabilizing	−0.057	Decrease of molecule flexibility
19	N856K	0.202, Destabilizing	1.304, Stabilizing	0.103, Stabilizing	0.314, Stabilizing	0.300, Destabilizing	−0.252	Decrease of molecule flexibility
20	Q498R	−0.289, Destabilizing	−0.163, Destabilizing	0.283, Stabilizing	0.519, Stabilizing	0.550, Stabilizing	0.361	Increase of molecule flexibility
21	S371L	*0.030,* Stabilizing	0.127, Stabilizing	−0.394, Destabilizing	0.080, Stabilizing	1.280, Stabilizing	−0.037	Decrease of molecule flexibility
22	G339D	−0.027, Stabilizing	0.019, Stabilizing	−0.69, Destabilizing	−0.400, Destabilizing	0.110, Stabilizing	0.033	Increase of molecule flexibility
23	L212I	−0.028, Destabilizing	0.090, Stabilizing	−0.844, Destabilizing	−0.334, Destabilizing	0.490, Stabilizing	0.035	Increase of molecule flexibility
24	S375F	0.578, Stabilizing	−0.125, Destabilizing	−0.948, Destabilizing	−0.460, Destabilizing	1.190, Stabilizing	−0.723	Decrease of molecule flexibility
25	S373P	−0.323, Destabilizing	−0.797, Destabilizing	−0.645, Destabilizing	−0.534, Destabilizing	−0.030, Destabilizing	0.404	Increase of molecule flexibility
26	N764K	−0.344, Destabilizing	0.189, Stabilizing	0.089, Stabilizing	0.475, Stabilizing	−0.300, Destabilizing	0.430	Increase of molecule flexibility
27	T547K	0.072, Destabilizing	0.462, Stabilizing	−0.244, Destabilizing	0.194, Stabilizing	−0.090, Destabilizing	−0.090	Increase of molecule flexibility
28	Q954H	0.192, Destabilizing	0.969, Stabilizing	−0.676, Destabilizing	−0.491, Destabilizing	0.060, Stabilizing	−0.240	Decrease of molecule flexibility

of the mutations (stabilizing, destabilizing, molecular flexibility) of RBD might augment the receptor-binding activity of Omicron, which might help to provide superior infectivity properties of Omicron. Our study has also attempted to understand the complete mutational landscape of Omicron along with the present VOCs and VOIs. It is important to understand the Omicron variant from a mutational point of view.

Emerging mutations in SARS-CoV-2 are a major concern for antibody escape, especially in nAb. Triveri et al. have attempted to describe the escape phenomena of SARS-CoV-2 variants because of mutations in the S-glycoprotein. They considered emerging variants such as the South African (501Y. V2), UK (B.1.1.7), Brazilian (P.1), and D614G variants to understand the correlation between the mutations and escape from immuno-recognition. The study also illustrated the ability of these variants to evade or decrease the recognition capacity of S-glycoprotein targeting antibodies [71]. However, we performed risk analysis for D614G antibody binding. We observed that the mutation in D614 has a high risk related to antibody-binding and can reduce the recognition capability by targeting antibodies to the S-glycoprotein. The outcome of our in silico risk analysis study of D614G corroborates the previous experimental study's result by Martin et al. [72]. Their study has found that the D614G mutation decreased antibody binding of the S-glycoprotein. Previously, we illustrated that the D614G variant is present in all VOCs and VOIs with high frequency, and the mutant variant may be a positive selection [28, 31, 32]. We are currently attempting to understand the prominent mutations in the S-glycoprotein in SARS-CoV-2 and their role in antibody escape [73, 74].

Several studies have shown that most antibodies bind closer to the NTD or RBD regions [75]. However, some RBD mutations are responsible for antibody escape [33, 34]. We evaluated some mutations, especially mutations in the RBD region in Omicron, and their probable consequence on antibody affinity [76]. In this study, we also attempted to evaluate some molecular and mutational properties of some mutations in the RBD region in Omicron, which may provide deeper insight into the mutations. We evaluated the molecular and mutational properties of some Omicron variants: G339D, S371L, N440K, G446S, T478K, and Q498R. Here, we describe the molecular and mutational properties of these mutations.

Recently, Singh et al. attempted to understand the ΔΔG between the wild-type and mutant proteins in *Mycobacterium tuberculosis*. We analyzed the ΔΔG value to understand the effects of mutations on molecular flexibility. Several researchers have computed ΔΔG values to understand the mutational properties of mutations in a human pathogen. It aids in the understanding of the properties of point mutations [77]. Othman et al. used the same algorithm to calculate the enthalpy (DDG) and entropy (DDS) to understand the folding energy during the interaction of the SARS-CoV-2 S-glycoprotein and host ACE2 [78]. We also calculated the ΔΔG of some point mutations (G339D, S371L, N440K, G446S, T478K, and Q498R), which are significant in the RBD region of the SARS-CoV-2 Omicron. We found fluctuation in the wild-type and mutant-type residues, atomic fluctuation in the wild-type and mutant-type S-glycoprotein, and deformation energies in the wild-type and mutant-type in the dynamics of the S-glycoprotein with respect to those mutations through the algorithms. Our analysis allowed us to illustrate the harmonic motions of the missense variants in terms of the S-glycoprotein through the analysis of ΔΔG values, which provides insights into accessible conformations of S-glycoprotein and its dynamics; however, we analyzed residue-wise RMS fluctuations, atomic fluctuations, and deformation energies of all mutations (G339D, S371L, N440K, G446S, T478K, and Q498R). The residue-wise RMS fluctuation (Figs. S2A, S3A, S4A, S5A, S6A, and S7A), atomic fluctuation (Figs. S2B, S3B, S4B, S5B, S6B, and S7B), and deformation energies (Figs. S2C, S3C, S4C, S5C, S6C, and S7C) of all these mutations showed a similar result in every category. Presently, scientists are attempting to understand the effects of spike-protein mutations on conformations and dynamics [79–81]. Our study illustrated the essential mutations of the Omicron variant.

The present study chose 28 mutations and six RBD mutations with immense importance in understanding the molecular properties of mutations. These RBD mutations may be associated with some significant properties of Omicron, such as antibody escape and ACE2 interaction. A schematic diagram was used to depict the mutation selection from the RBD region of the S-glycoprotein (Fig. 1B). Finally, we attempted to evaluate all 28 mutations, including the six RBD mutations, to understand mutational properties such as stabilizing or destabilizing events and increased or decreased molecular flexibility.

The study performed a comparative analysis of ΔΔG of the 28 mutations of the S-glycoprotein, including the six RBD mutations, to understand the stabilizing or destabilizing properties and other mutational properties. The comparative outcome is noted in Table 5. ΔΔG analysis and the stabilizing

or destabilizing properties were analyzed using the DynaMut server and other mutational properties. We chose six mutations in the RBD of Omicron for a more detailed analysis, G339D, S371L, N440K, G446S, T478K, and Q498R. The research outcome of the six RBD mutations showed that G339D, S371L, N440K, and T478K were stable with 0.019 kcal/mol and 0.127 kcal/mol, 0.064 kcal/mol, and 1.009 kcal/mol, respectively. Other mutations (G446S and Q498R) showed destabilizing results (Fig. 21A). It is noteworthy that, among the six RBD mutations, G339D, G446S, and Q498R mutations increased the molecular flexibility of the S-glycoprotein (Fig. 21B). These RBD mutations may help RBD interact with the ACE2 receptor, thus helping to increase Omicron infectivity. Our study aids future researchers in understanding the mutational landscape of Omicron and in elucidating more about the different properties of Omicron, such as infectivity and antibody escape, using our analyzed properties (stabilizing or destabilizing as well as increased or decreased molecular flexibility of the S-glycoprotein to interact with the mAb/receptor) of those using the 28 emerging mutations along with six RBD mutations. Recently, several researchers have characterized SARS-CoV-2 mutations using the DynaMut server. The DDG of some mutations (L452R, E484Q, and P681R) in the Indian variant (B.1.617) was computed using the DynaMut server [82]. Another study characterized three mutations in an Italian SARS-CoV-2 strain using the DynaMut server [83]. This study analyzed the properties of 28 mutations, including six RBD mutations of the Omicron variant, in a short time. This information may be essential supportive data for future researchers who further unfold the significant properties of Omicron and other VOCs and provide a solution to the pandemic. From this perspective, our study is highly important.

Limitations

The Omicron variant is a crucial variant termed by the WHO as a VOC because of its infectivity, antibody escape, and partial vaccine escape. Therefore, this variant has created a more challenging pandemic [65, 74, 76, 84]. In this study, we evaluated 28 mutations in Omicron and their properties. The study computed the increased or decreased stability event and the increased or decreased molecular flexibility of the S-glycoprotein because of the mutational change using the DynaMut server in a short time. This may be a limitation of the present study. However, this paper presents a more detailed analysis of these eight mutations. Simultaneously, we computed different data using bioinformatics tools and servers. We cannot calculate some data, such as AA variants of ORF6. This may be another limitation of this study. However, this computational experiment with the mutation of the S-glycoprotein, especially in the RBD region, will help understand the ACE2 binding ability of Omicron and, thus, infectivity. The results generated in a short time frame will also help understand Omicron's antibody escape properties. Our rapidly generated data may be helpful for future research from a pandemic perspective because the Omicron variant is a VOC.

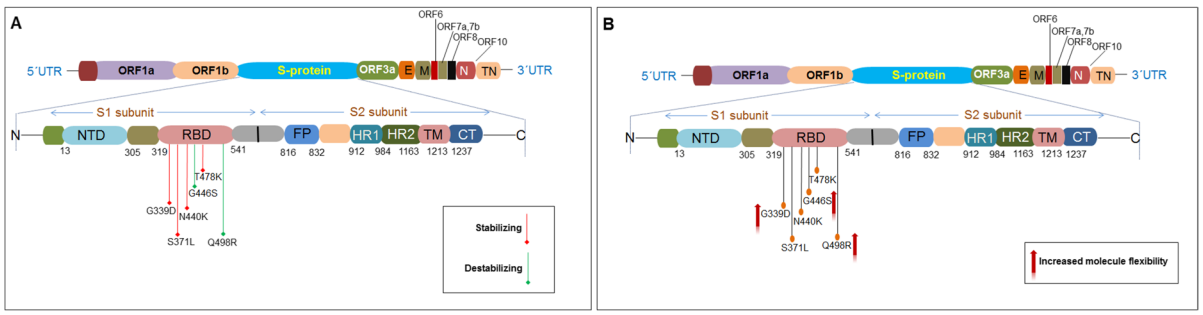

Fig. 21 The graphical image shows the emerging mutations of RBD (S-glycoprotein) of the Omicron. It is also shown how it affects flexibility changes and stability alteration due to amino acid point mutation. (**A**) The schematic diagram illustrates the emerging mutations of RBD (S-glycoprotein) of the Omicron and their effects on stability (stabilizing event or destabilizing) (**B**) The schematic diagram shows the emerging mutations of RBD (S-glycoprotein) of the Omicron and their impact on flexibility

Conclusion

The present study represents the mutational landscape of the Omicron variant along with the emerging VOCs and VOIs, which helps us to understand the pattern of Omicron mutations in the whole genome in terms of SNVs along with the AA variants of structural proteins and non-structural proteins. The study also revealed some molecular properties of the mutations, such as increased or decreased stability events and the increased or decreased molecular flexibility of the S-glycoprotein because of the mutational change.

In this study, we applied computational servers and tools to explain the mutational landscape of the Omicron variant, a newly emerging SARS-CoV-2 variant, and compared the mutations with those in current VOCs and VOIs. In this study, we evaluated all the emerging mutations and categorized them in terms of mutational frequency.

The stability of the S-glycoprotein depends on the different stable mutations, and all the mutations in the region determine the interaction capacity with the host receptor binding and its stability. This study noted that 19 mutations showed stabilizing effects based on the ΔΔG prediction of 28 mutations. Conversely, mutations affect the stability of the S-glycoprotein, which may play a significant role in receptor recognition, increasing infectivity, and improving viral fitness. This study also observed that 12 mutations increased the molecular flexibility and flexibility of the S-glycoprotein. It may play a significant role in receptor binding, increasing infectivity, and improving viral fitness.

Our study also analyzed the mutational frequency of all AA variants in all structural and non-structural proteins of SARS-CoV-2. This study may help future researchers to understand the stability of all the proteins of SARS-CoV-2. Therefore, our study can help future researchers understand the Omicron variant's fast-spreading properties. Our study attempted to illustrate the molecular and mutational properties of the emerging mutations in the RBD regarding nAb interaction and escape. Furthermore, our study comprehensively mapped RBD mutations in terms of several molecular and mutational parameters, such as ΔΔG, interatomic interactions in the wild-type and mutant-type residues, and fluctuation and deformation analysis. The study will help future researchers to understand the antigenic properties of epitopes of the S-glycoprotein. Finally, this study will help future researchers design and develop novel vaccines and therapeutic antibodies using the SNVs and point mutations with high frequencies in the case of all VOIs and VOCs, including Omicron.

Author contribution CC conceptualized the study, collected and analyzed the data, and wrote the manuscript. MB did the formal analysis and developed the figures and tables. ARS reviewed and edited the final draft of the manuscript. GA edited the manuscript. KD and CC did the overall supervision. All authors read and approved the manuscript.

Availability of data and materials All data generated or analyzed during this study are included in this published article (and its supplementary information files).

Declarations

Ethics approval and consent to participate Not applicable.

Consent for publication Not applicable.

Competing interests The authors declare no competing interests.

References

1. Vaughan A. Omicron emerges. New Sci. 2021;252(3363):7.
2. Dyer O. Covid-19: South Africa's surge in cases deepens alarm over omicron variant. BMJ. 2021;3(375): n3013.
3. Karim SSA, Karim QA. Omicron SARS-CoV-2 variant: a new chapter in the COVID-19 pandemic. The Lancet. 2021;398(10317):2126–8.
4. Rathinasamy M, Kandhasamy S. An exploratory study on the propagation of SARS-CoV-2 variants: Omicron is the most predominant variant. J Med Virol. 2022;94(6):2414–21.
5. Abbasi J. Omicron has reached the US—here's what infectious disease experts know about the variant. JAMA. 2021;326(24):2460–2.
6. Graham F. Daily briefing: Omicron was already spreading in Europe. Nature. 2021. https://doi.org/10.1038/d41586-021-03610-3.
7. Mohapatra RK, et al. Omicron (B. 11. 529) variant of SARS-CoV-2: concerns, challenges, and recent updates. J Med Virol. 2022;94(6):2336–42.
8. Mohapatra RK, et al. The recently emerged BA. 4 and BA. 5 lineages of Omicron and their global health concerns amid the ongoing wave of COVID-19 pandemic—correspondence. Int J Surg. 2022;103:106698.
9. Fan Y, et al. SARS-CoV-2 Omicron variant: recent progress and future perspectives. Signal Transduct Target Ther. 2022;7(1):1–11.

10. Chakraborty C, et al. Recombinant SARS-CoV-2 variants XD, XE, and XF: the emergence of recombinant variants requires an urgent call for research—correspondence. Int J Surg. 2022;2022(102): 106670.
11. WHO. Tracking SARS-CoV-2 variants. 2022. https://www.who.int/activities/tracking-SARS-CoV-2-variants. Acessed on 13 July 2022.
12. Singh J, et al. Evolutionary trajectory of SARS-CoV-2 and emerging variants. Virol J. 2021;18(1):1–21.
13. Jung C, et al. Omicron: what makes the latest SARS-CoV-2 variant of concern so concerning? J Virol. 2022;96(6):e02077-e2121.
14. Desvars-Larrive A. To beat Omicron, Delta and bird flu, Europe must pull together. Nature. 2021;600(7889):386–386.
15. McKee M. Public health and politics are inseparable, as Omicron and the UK's response remind us. BMJ. 2021;375: n3055.
16. Zhang L, et al. The significant immune escape of pseudotyped SARS-CoV-2 variant Omicron. Emerg Microb Infect. 2022;11(1):1-5.12.
17. Callaway E. Omicron likely to weaken COVID vaccine protection. Nature. 2021;600(7889):367–8.
18. Zhang X, et al. SARS-CoV-2 Omicron strain exhibits potent capabilities for immune evasion and viral entrance. Signal Transduct Target Ther. 2021;6(1):1–3.
19. Quarleri J, Galvan V, Delpino M. Omicron variant of the SARS-CoV-2: a quest to define the consequences of its high mutational load. Geroscience. 2021;44(1):53–6.
20. Kumar S, et al. Omicron and Delta variant of SARS-CoV-2: a comparative computational study of spike protein. J Med Virol. 2022;94(4):1641–9.
21. Pascarella S, et al. The electrostatic potential of the omicron variant spike is higher than in delta and delta-plus variants: a hint to higher transmissibility? J Med Virol. 2022;94(4):1277–80.
22. Chan JFW, Chu H. Pathogenicity of SARS-CoV-2 Omicron BA. 1.1 in hamsters. eBioMedicine. 2022;80:104035.
23. Mohapatra RK, et al. The recombinant variants of SARS-CoV-2: concerns continues amid COVID-19 pandemic. J Med Virol. 2022. https://doi.org/10.1002/jmv.27780.
24. Scott L, et al. Track Omicron's spread with molecular data. Science. 2021;374(6574):1454–5.
25. Callaway E. Heavily mutated Omicron variant puts scientists on alert. Nature. 2021;600(7887):21–21.
26. Song Y, Masaki F. Preparation for the challenge of heavily mutated Omicron variant. Clin Transl Med. 2021;11(12):e679. https://doi.org/10.1101/2021.12.06.471499.
27. Miller NL, et al. Insights on the mutational landscape of the SARS-CoV-2 Omicron variant. bioRxiv, 2021.
28. Chakraborty C, et al. Evolution, mode of transmission, and mutational landscape of newly emerging SARS-CoV-2 variants. MBio. 2021;12(4):e01140-e1221.
29. Chakraborty C, Bhattacharya M, Sharma AR. Present variants of concern and variants of interest of severe acute respiratory syndrome coronavirus 2: their significant mutations in S-glycoprotein, infectivity, re-infectivity, immune escape and vaccines activity. Rev Med Virol. 2021;32(2):e2270. https://doi.org/10.1002/rmv.2270
30. Chakraborty C, et al. SARS-CoV-2 Brazil variant in Latin America: more serious research urgently needed on public health and vaccine protection. Ann Med Surg. 2021;66:102428.
31. Bhattacharya M, et al. D614G mutation and SARS-CoV-2: impact on S-protein structure, function, infectivity, and immunity. Appl Microbiol Biotechnol. 2021;105(24):9035–45.
32. Chakraborty C, et al. D614G mutation eventuates in all VOI and VOC in SARS-CoV-2: is it part of the positive selection pioneered by Darwin? Mol Ther- Nucleic Acids. 2021;26(3):237–41.
33. Yang L, et al. SARS-CoV-2 variants, RBD mutations, binding affinity, and antibody escape. Int J Mol Sci. 2021;22(22):12114.
34. Greaney AJ, et al. Mapping mutations to the SARS-CoV-2 RBD that escape binding by different classes of antibodies. Nat Commun. 2021;12(1):1–14.
35. Farooq RK, et al. Bibliometric analysis of coronavirus disease (COVID-19) literature published in Web of Science 2019–2020. J Fam Community Med. 2021;28(1):1.
36. Thoma B, Chan TM. Using Google Scholar to track the scholarly output of research groups. Perspect Med Educ. 2019;8(3):201–5.
37. Zuo X, et al. How do we share data in COVID-19 research? A systematic review of COVID-19 datasets in PubMed Central Articles. Brief Bioinform. 2021;22(2):800–11.
38. Chan J, et al. COVID-19 and literature evidence: should we publish anything and everything? Acta Bio Med: Atenei Parmensis. 2020;91(3): e2020020.
39. CDC. Omicron variant: what you need to know. 2021. https://www.cdc.gov/coronavirus/2019-ncov/variants/omicron-variant.html. Acessed on 12 Jan 2022.
40. CDC. Science brief: Omicron (B.1.1.529) variant. 2021. https://www.cdc.gov/coronavirus/2019-ncov/science/science-briefs/scientific-brief-omicron-variant.html. Acessed on 12 Jan 2022.
41. Stockholm E. Implications of the spread of the SARS-CoV-2 B.1.1.529 variant of concern (Omicron) for the EU/EEA—first update. 2 December 2021. 2021.
42. WHO. Update on Omicron. 2021. https://www.who.int/news/item/28-11-2021-update-on-omicron. Acessed on 5 Jan 2022.
43. Shu Y, McCauley J. GISAID: Global initiative on sharing all influenza data—from vision to reality. Eurosurveillance. 2017;22(13):30494.
44. Elbe S, Buckland-Merrett G. Data, disease and diplomacy: GISAID's innovative contribution to global health. Global Chall. 2017;1(1):33–46.
45. Velankar S, et al. The protein data bank archive. Methods Mol Biol. 2021;2305:3–21.
46. Yuan S, et al. PyMOL and Inkscape bridge the data and the data visualization. Structure. 2016;24(12):2041–2.
47. Rigsby RE, Parker AB. Using the PyMOL application to reinforce visual understanding of protein structure. Biochem Mol Biol Educ. 2016;44(5):433–7.
48. Chen AT, et al. COVID-19 CG enables SARS-CoV-2 mutation and lineage tracking by locations and dates of interest. Elife. 2021;10: e63409.

49. Mathieu E, et al. A global database of COVID-19 vaccinations. Nat Hum Behav. 2021;5(7):947–53.
50. Nextstrain. Nextstrain SARS-CoV-2 resources, on Nextstrain. 2021. https://nextstrain.org/sars-cov-2/. Acessed on 5 Jan 2022.
51. Karthik Gangavarapu et al. Outbreak.info genomic reports: scalable and dynamic surveillance of SARS-CoV-2 variants and mutations. 2022. https://doi.org/10.1101/2022.01.27.22269965.
52. Sun Q, et al. VarEPS: an evaluation and prewarning system of known and virtual variations of SARS-CoV-2 genomes. Nucleic Acids Res. 2021;50(D1):D888–D897.
53. Rodrigues CH, Pires DE, Ascher DB. DynaMut: predicting the impact of mutations on protein conformation, flexibility and stability. Nucleic Acids Res. 2018;46(W1):W350–5.
54. Capriotti E, et al. A three-state prediction of single point mutations on protein stability changes. BMC Bioinformatics. 2008;9(2):1–9.
55. Hammer Ø, Harper DA, Ryan PD. PAST: Paleontological statistics software package for education and data analysis. Palaeontol Electron. 2001;4(1):9.
56. MathWorks I. MATLAB, High-performance numeric computation and visualization software: user's guide: for UNIX Workstations. MathWorks; 1992.
57. Kwon D. Omicron's molecular structure could help explain its global takeover. Nature. 2022;602(7897):373–4.
58. Yadav PD, et al. Isolation and genomic characterization of SARS-CoV-2 omicron variant obtained from human clinical specimens. Viruses. 2022;14(3):461.
59. Ahmed W, et al. Detection of the Omicron (B. 1.1. 529) variant of SARS-CoV-2 in aircraft wastewater. Sci Total Environ. 2022;10(820):153171.
60. Nikolaidis M, et al. Comparative Analysis of SARS-CoV-2 Variants of concern, including Omicron, highlights their common and distinctive amino acid substitution patterns, especially at the spike ORF. Viruses. 2022;14(4):707.
61. Zhang Y, et al. Cross-species tropism and antigenic landscapes of circulating SARS-CoV-2 variants. Cell Rep. 2022;38(12): 110558.
62. Mercatelli D, Giorgi FM. Geographic and genomic distribution of SARS-CoV-2 mutations. Front Microbiol. 2020;11:1800.
63. Korber B, et al. Tracking changes in SARS-CoV-2 spike: evidence that D614G increases infectivity of the COVID-19 virus. Cell. 2020;182(4):812–27.
64. Khairnar P, et al. Recent highlights on Omicron as a new SARS-COVID-19 variant: evolution, genetic mutation and future perspectives. J Drug Target. 1–33. https://doi.org/10.1080/1061186X.2022.2056187.
65. Dong E, Du H, Gardner L. An interactive web-based dashboard to track COVID-19 in real time. Lancet Infect Dis. 2020;20(5):533–4.
66. Cui Z, et al. Structural and functional characterizations of infectivity and immune evasion of SARS-CoV-2 Omicron. Cell. 185(5):860–871.
67. Planas D, et al. Considerable escape of SARS-CoV-2 Omicron to antibody neutralization. Nature. 2022;602(7898):671–5.
68. Jacob JJ, et al. Evolutionary tracking of SARS-CoV-2 genetic variants highlights an intricate balance of stabilizing and destabilizing mutations. MBio. 2021;12(4):e01188-e1221.
69. Islam MR, Hossain MJ. Detection of SARS-CoV-2 Omicron (B.1.1.529) variant has created panic among the people across the world: what should we do right now? J Med Virol. 2022;94(5):1768–9.
70. Lupala CS, et al. Mutations on RBD of SARS-CoV-2 Omicron variant result in stronger binding to human ACE2 receptor. Biochem Biophys Res Commun. 2021;29(590):34–41.
71. Triveri A, et al. SARS-CoV-2 spike protein mutations and escape from antibodies: a computational model of epitope loss in variants of concern. J Chem Inf Model. 2021;61(9):4687–700.
72. Martin S, et al. SARS-CoV-2 integral membrane proteins shape the serological responses of patients with COVID-19. Iscience. 2021;24(10): 103185.
73. Chakraborty C, Bhattacharya M, Sharma AR. Emerging mutations in the SARS-CoV-2 variants and their role in antibody escape to small molecule-based therapeutic resistance. Curr Opin Pharmacol. 2022;62:64–73.
74. Chakraborty C, et al. A detailed overview of immune escape, antibody escape, partial vaccine escape of SARS-CoV-2 and their emerging variants with escape mutations. Front Immunol. 2022;13:801522–801522.
75. Liu L, et al. Potent neutralizing antibodies against multiple epitopes on SARS-CoV-2 spike. Nature. 2020;584(7821):450–6.
76. Bhattacharya M, et al. Omicron variant (B. 1.1. 529) of SARS-CoV-2: understanding mutations in the genome, S-glycoprotein, and antibody-binding regions. GeroScience. 2022;44(2):619–37.
77. Singh P, et al. Computational modeling and bioinformatic analyses of functional mutations in drug target genes in Mycobacterium tuberculosis. Comput Struct Biotechnol J. 2021;19:2423–46.
78. Othman H, et al. Interaction of the spike protein RBD from SARS-CoV-2 with ACE2: similarity with SARS-CoV, hot-spot analysis and effect of the receptor polymorphism. Biochem Biophys Res Commun. 2020;527(3):702–8.
79. Sixto-López Y, et al. Structural insights into SARS-CoV-2 spike protein and its natural mutants found in Mexican population. Sci Rep. 2021;11(1):1–16.
80. Teng S, et al. Systemic effects of missense mutations on SARS-CoV-2 spike glycoprotein stability and receptor-binding affinity. Brief Bioinform. 2021;22(2):1239–53.
81. Begum F, et al. Analyses of spike protein from first deposited sequences of SARS-CoV2 from West Bengal, India. F1000Research. 2020;9:371.
82. Pascarella S, et al. SARS-CoV-2 B. 1.617 Indian variants: are electrostatic potential changes responsible for a higher transmission rate? J Med Virol. 2021;93(12):6551–6.

83. Benvenuto D, et al. Analysis of three mutations in Italian strains of SARS-CoV-2: implications for pathogenesis. Chemotherapy. 2021;66(1–2):33–7.
84. Shao W, et al. Challenges and countermeasures brought by Omicron Variant. J Microbiol Immunol Infect. 2022;S1684–1182(22):00054–8.